International Journal of Nanomedicine

Dovepress
Taylor & Francis Group

Open Access Full Text Article

ORIGINAL RESEARCH

DS-Modified Paeoniflorin pH-Responsive Lipid–Polymer Hybrid Nanoparticles for Targeted Macrophage Polarization in a Rat Model of Rheumatoid Arthritis

Junhao Zhang[1,*], Jing Yang[2,*], Zhoubo Yu[1], Haotian Bai[1], Yanhong Wang[1,3], Rui Wang[1,3]

[1]College of Pharmacy, Heilongjiang University of Chinese Medicine, Harbin, Heilongjiang, 150040, People's Republic of China; [2]Basic Medical College, Heilongjiang University of Chinese Medicine, Harbin, Heilongjiang, 150040, People's Republic of China; [3]Key Laboratory of Basic and Application Research of Beiyao, Heilongjiang University of Chinese Medicine, Ministry of Education, Harbin, Heilongjiang, 150040, People's Republic of China

*These authors contributed equally to this work

Correspondence: Rui Wang; Yanhong Wang, College of Pharmacy, Heilongjiang University of Chinese Medicine, Wenzheng Street, Harbin, Heilongjiang, 150040, People's Republic of China, Tel/Fax +86-0451-87266893, Email wrdx@sina.com; wang.yanhong@163.com

Purpose: Macrophages play a pivotal role in rheumatoid arthritis (RA) pathogenesis. Paeoniflorin, a traditional Chinese medication, reduces inflammation by suppressing immune cell activation and inducing synovial fibroblast apoptosis, attenuating RA disease progression. Despite the potential therapeutic benefits, free paeoniflorin has limitations, including low drug utilization, poor selectivity, and short half-life during administration. We aimed to develop and evaluate dextran sulfate-modified paeoniflorin pH-responsive lipid–polymer hybrid nanoparticles (Pae–PPNPs–DS) for targeted macrophage delivery and improved treatment efficacy in RA. The pH sensitivity is attributed to the incorporation of poly(cyclohexane-1,4-dimethylene ketal), which undergoes hydrolysis-triggered degradation under acidic conditions enabling passive targeting to inflammatory sites through pH-dependent drug release. Simultaneously, dextran sulfate serves as a ligand to actively target Scavenger receptor class A type I overexpressed on activated macrophages in RA synovium, achieving dual-targeted delivery via environmental responsiveness and ligand-receptor interaction.

Methods: We developed dextran sulfate-modified Pae–PPNPs–DS, which exhibits dual capabilities of active macrophage targeting and pH-triggered drug release, to deliver paeoniflorin to macrophages and improve drug delivery at the joint inflammation site. Nanoparticle characterization, in vitro release behavior, stability, macrophage uptake, macrophage polarization pathway, phenotypic polarization, and therapeutic efficacy were evaluated in a rat model of RA.

Results: Pae–PPNPs–DS had smooth surfaces, uniform particle sizes, physical stability, and pH-responsive characteristics. RAW264.7 macrophages showed enhanced Pae–PPNPs–DS uptake. Pae–PPNPs–DS effectively modulated the STAT signaling pathway and modulated macrophage polarization. Pae–PPNPs–DS inhibited the expression of *TNF-α*/*IL-1β*/*iNOS*/*IL-6* (pro-inflammatory and M1 markers), while promoting *IL-10*/*Arg-1*/*TGF-β* (anti-inflammatory and M2 markers) secretion. Pathological analysis revealed that Pae–PPNPs–DS prevented synovial tissue proliferation, inhibited inflammatory cell infiltration, and exhibited therapeutic efficacy.

Conclusion: Pae–PPNPs–DS actively target macrophages, regulate polarization through STAT pathway, and inhibit joint inflammation, suggesting its potential in treating RA. The study highlights the potential of pH-responsive nanocarriers as an innovative approach to treating autoimmune diseases.

Plain Language Summary: Rheumatoid arthritis (RA) is a chronic condition that causes painful swelling and damage to the joints and is driven in part by overactive immune cells called macrophages, which produce harmful inflammation. Current treatments for RA can be expensive and have significant side effects, highlighting the need for new, safer therapies. Our study focused on improving how a natural compound called paeoniflorin is delivered to the inflamed joints of people with RA. Paeoniflorin has anti-inflammatory properties, but it does not last long in the body and is not very effective on its own. To address this, we developed tiny, specially designed carriers called nanoparticles to deliver paeoniflorin directly to the inflamed areas of the joints. These nanoparticles are coated with a material that helps them target macrophages and release the drug when they reach the acidic environment of the inflamed tissue. We tested our nanoparticles

Received: 8 January 2025
Accepted: 9 June 2025
Published: 12 July 2025

in vitro and in vivo with RA-like symptoms. The results were promising: the nanoparticles were endocytosed by macrophages, reduced harmful inflammation, and promoted healing. In rats, these nanoparticles reduced joint swelling and tissue damage more effectively than the drug on its own. They also showed good safety and stability. These findings suggest that this new delivery system could be a more effective and targeted way to treat RA, reducing the inflammation and pain caused by the disease while avoiding some of the side effects of current treatments. This approach could lead to better outcomes for people living with RA.

Keywords: hybrid nanoparticles, macrophage targeting, pH-responsive drug delivery, targeted therapy, CIA model

Introduction

Rheumatoid arthritis (RA), a chronic autoimmune disease with a prevalence of 0.5–1.0%, is characterized by synovitis and progressive joint destruction.[1] While the advent of biologics/small-molecule inhibitors has advanced RA treatment, their high cost impedes their application.[2,3] Consequently, antirheumatic/nonsteroidal anti-inflammatory drugs and glucocorticoids remain the preferred treatment for RA in clinical settings; however, these drugs have non-negligible adverse effects, particularly cardiovascular complications and systemic toxicity that exacerbate therapeutic resistance due to nonspecific biodistribution.[4,5] Although the etiology of RA remains uncertain, activated macrophages can promote inflammatory factor secretion and exacerbate joint damage.[6,7] Significantly, Scavenger receptor class A type I (SR-AI) is pathologically overexpressed on the surface of activated macrophages offering a therapeutic leverage point to bypass drug resistance mechanisms while minimizing off-target organ exposure. Regulating macrophage polarization through SR-AIs could help alleviate RA. These findings indicate the importance of establishing safe and effective dual-targeting delivery systems that simultaneously alleviates the therapeutic resistance and systemic toxicity in RA treatment, while targeting minimal toxicity of inflammatory joint tissues for treating RA.

Traditional Chinese medicine has long been used to treat RA. *Paeonia lactiflora* contains various active compounds that offer a multi-targeted therapy with relatively fewer side effects, thereby garnering increased attention. Paeoniflorin, the main constituent of *P. lactiflora*, has anti-inflammatory, analgesic, and immunomodulatory effects.[8] Paeoniflorin reduces inflammation by activating immune cells and inducing synovial fibroblast apoptosis, thus attenuating disease progression.[9–12] However, its efficacy is limited by low bioavailability,[13] which can be circumvented by structural modifications/drug interactions.[14]

Lipid–polymer hybrid nanoparticles (LPNs) are seamless core-shell nanoparticles comprising a hydrophobic polymer core encased in a lipid shell. LPNs possess the stability of polymer nanoparticles and liposomes, overcoming the limitations of the two nanodrug delivery systems. For instance, liposomes often face challenges such as rapid drug leakage, short storage stability, and rapid clearance by the reticuloendothelial system (RES), whereas polymeric nanoparticles face challenges, such as colloidal instability, complex synthesis processes, potential toxicity, and difficulties in large-scale production. In contrast, LPNs combine the structural robustness of a polymer core for enhanced drug encapsulation efficiency and controlled release with a lipid shell that improves biocompatibility and reduces RES recognition. This unique architecture allows the lipid layer to optimize biomembrane permeability, while the porous polymer network within the core enables precise redistribution of the released drug. Surface-targeted modification enhances their biocompatibility, while the polymer core improves drug encapsulation.[15,16] Dextran sulfate (DS) is a polyanion ligand of SR-AI. Poly(cyclohexane-1,4-dimethylene ketal) (PCADK) is a biocompatible synthetic polyketal that undergoes safe, non-toxic degradation. Its rapid degradation (pH 4.5) and short half-life are highly useful.[17] Cytokines play pivotal roles in the pathogenesis of RA. *TNF-α*/*IL-1β*/*iNOS*/*IL-6* are pro-inflammatory markers of M1 macrophages, whereas *IL-10*/*Arg-1*/*TGF-β* is an anti-inflammatory marker of M2 macrophages.[18]

Nano-delivery systems that can target macrophage activation and precisely deliver drugs to joint inflammation are current hotspots in RA treatment. Here, we developed a novel nanomedicine particle comprising poly(lactic-co-glycolic acid) (PLGA), PCADK, modified DS with 1,2-dioleoyl-3-trimethylammonium propane (DOTAP), DS, and lipids encapsulated in paeoniflorin (Figure 1). In this study, we aimed to target macrophages using structural modifications of lipid–polymer nanoparticles. For this, DS is incorporated into the nanocarrier to target SR-AI, which is overexpressed on macrophages. PCADK was included for its acid-sensitive properties that facilitate nanoparticle reaggregation at the site of inflammation by leveraging the acidic microenvironment of the RA joints. The sustained and localized acidosis in

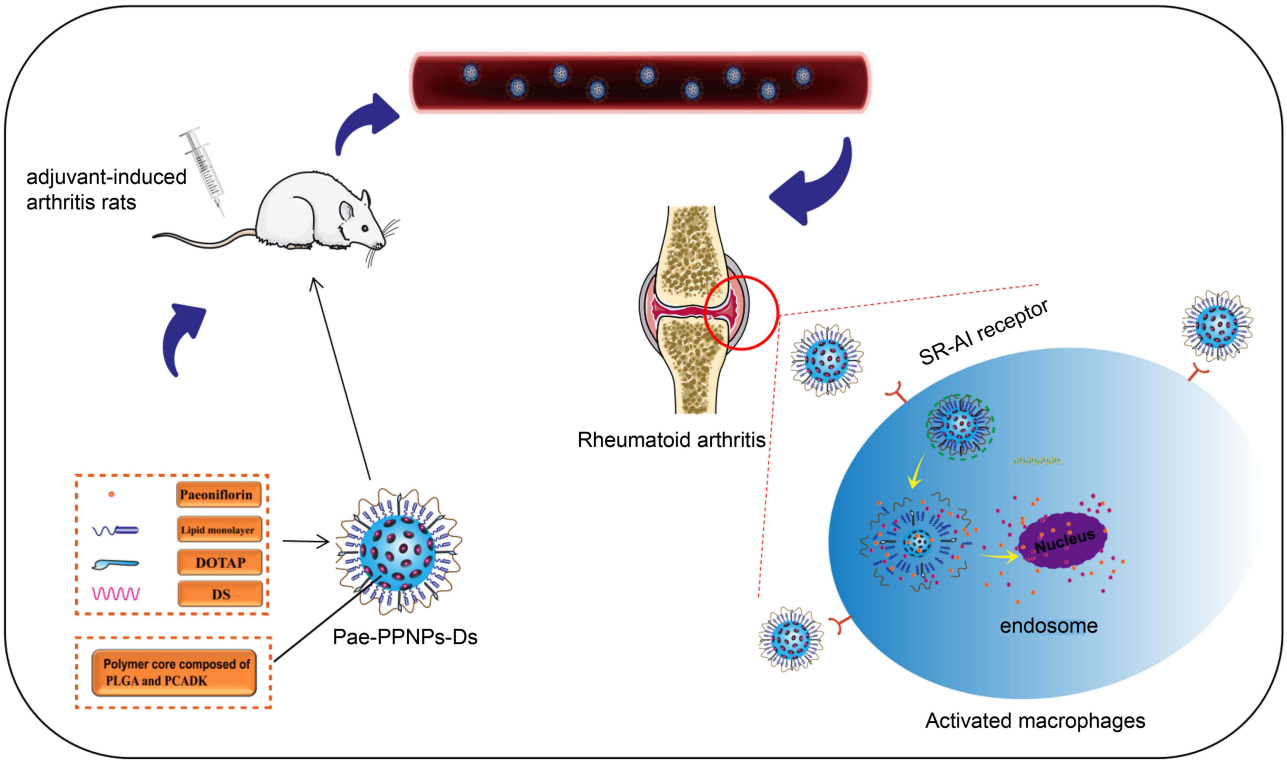

Figure 1 Schematic of the mechanism of Pae–PPNPs–DS in treating rheumatoid arthritis.
Abbreviations: DOTAP, 1,2-dioleoyl-3-trimethylammonium propane; DS, dextran sulfate; PCADK, Poly(cyclohexane-1,4-dimethylene ketal); PLGA, poly(lactic-co-glycolic acid); Pae–PPNPs–DS, DS-modified paeoniflorin pH-responsive lipid–polymer hybrid nanoparticles; SR-AI, scavenger receptor class A type I.

the RA synovial fluid provides a more reliable and disease-specific stimulus for triggered drug delivery. Meanwhile, lipids improve biocompatibility. We adjusted the ratio of each component to successfully develop paeoniflorin-loaded DS-targeted pH-responsive nanoparticles (Pae–PPNPs–DS) with a uniform particle size distribution, stable potential, and adequate drug-loading (DL) capacity. Polymer lipid hybrid nanoparticles combine the advantages of liposomes and polymer nanoparticles, regulate the redistribution of Pae released from the inner core, and improve the stability, tissue specificity, retention, and biofilm permeability of Pae. Therefore, we believe that Pae–PPNPs–DS can enhance the therapeutic effect by accumulating in the area of joint inflammation and damaged tissue. In addition, unlike the monotherapy for RA, the combination of targeted drug delivery and macrophage polarization regulation therapy in this study brings hope for perfecting the RA treatment scheme, ultimately achieving better patient treatment outcomes.

Materials and Methods

Details on the key reagents and instrumentation are available in the Supplementary Tables S1 and S2.

Nanoparticle Preparation

For precise delivery to the site of joint inflammation, PCADK was synthesized/fabricated according to the previously reported method;[19] paeoniflorin was encapsulated with PLGA, egg-yolk lecithin, PCADK, and modified DS with DOTAP to modulate charge, obtaining targeted macrophage-activated Pae–PPNPs–DS. In some experiments, the requisite quantity of paeoniflorin (s31585; Yuanye Biotechnology Co. Ltd.) was weighed and dissolved to prepare the organic-phase solution in 100% ethanol. PLGA (APB012; AmyJet Scientific Inc.), PCADK (made in-house), egg-yolk lecithin (s30871; Yuanye Biotechnology Co. Ltd.), and DOTAP (Q01001; Highfine Biotech Co. Ltd.) were dissolved in dichloromethane, and the two solutions were combined. In an ice bath (4°C), 1% polyvinyl alcohol was infused into the organic-phase solution to obtain an emulsion. After ultrasonic treatment with a 300-W probe (3 min), ultrapure water (15 mL) was added. The mixture was magnetically stirred (5 h) to create a suspension. DS solution was added dropwise and mixed (8 h). Nanoparticles were filtered through a 0.45-μm aqueous

membrane, centrifuged at 10,000 rpm (10 min), and thrice washed with ultrapure water. Freeze-dried Pae–PPNPs–DS powder was stored at 4°C.

Establishment of an in vitro Assay for Pae–PPNPs–DS

Details on the Chromatographic conditions, solution preparation, specificity, linear relationship, precision, repeatability, stability and sample recovery are available in the Supplementary Data.

Nanoparticle Characterization

Freshly prepared Pae–PPNPs–DS were diluted 10-fold. The average diameter, polydispersity index (PDI), and zeta potential were measured using a Nano-ZS90 particle size analyzer (Malvern Panalytical Instruments). Drug loading (DL) and encapsulation efficiency (EE) were ascertained using an H-Class Ultra-Performance Liquid Chromatography system (e2695; Waters).

EE (%) and DL (%) were calculated as follows:

$$EE(\%) = \frac{amout\ of\ input\ amount\ of\ paeoniflorin\ in\ supernatant}{amout\ of\ paeoniflorin\ input} Ga€''100\%$$

$$DL(\%) = \frac{quality\ of\ paeoniflorin}{quality\ of\ nanoparticles} Ga€''100\%$$

Nanoparticle Stability

Pae–PPNPs–DS were prepared at a concentration of 1 mg/mL in ultrafiltration centrifugal tubes with a cut-off capacity of 100 kDa. To simulate in vitro and in vivo environments, Pae–PPNPs–DS were incubated in phosphate-buffered saline (PBS) (pH 7.4) (WH0112201911XP; Pricella Biotechnology Co. Ltd.), at 25°C, and in PBS containing 10% fetal bovine serum (FBS) (pH 7.4), at 37°C. Particle size and zeta potential were measured at 0/12/24/48 h.

In vitro pH Sensitivity

In vitro patterns and pH sensitivity of Pae–PPNPs–DS in media with different pH values were analyzed by dialysis. Freshly prepared Pae–PPNPs–DS (3 mL) were sealed in dialysis bags, placed in PBS (50 mL; pH 5.0/7.4), and incubated at 37°C in a shaker. At 0/4/8/12/24/48 h, the release solution was collected and replenished with an equal volume of release medium at the same temperature. Paeoniflorin concentration was determined using high-performance liquid chromatography (HPLC).

Cell Culture

RAW264.7 macrophages were cultured in RAW264.7 cell-specific medium (CM-0190; Pricella Biotechnology Co. Ltd.) containing 10% FBS at 37°C/5% CO_2.

Cytotoxicity

Pae–PPNPs–DS safety was evaluated using the MTT assay. Lipopolysaccharide (LPS) (1 μg/mL)-activated macrophages and normal macrophages cultured in 96-well plates (1×10^5 cells/well) were treated with Pae–PPNPs–DS or PPNPs–DS, respectively. After 24 h, their cellular activity was determined by MTT staining whose absorbance was measured at 570 nm using a SPARK 10M Microplate Reader.

Apoptosis

The effects of various drugs/drug-loaded nanoparticles on the apoptosis of LPS-induced RAW264.7 macrophages were assessed using flow cytometry. Flow cytometry was conducted following double staining with Annexin V-FITC/Propidium iodide (PI). RAW264.7 macrophages (3×10^5) were inoculated into a 6-well plate. Control (treated with complete medium), LPS (treated with 1 μg/mL LPS), and paeoniflorin/Pae–PPNPs/Pae–PPNPs–DS groups (treated with

the corresponding drug at a final concentration of 1 μg/mL LPS) were incubated for 24 h. After Annexin V-FITC conjugate solution (200 μL) and Annexin V-FITC staining solution (5 μL) were added, followed by incubation in the dark at 25°C (30 min). Cells were added with PI (10 μL) in an ice bath, followed by incubation in the dark at 25°C (3 min) (C1062S; Biotime Biotechnology). Apoptosis was assessed using a Guava EasyCyte flow cytometer (Luminex).

Acridine Orange/Ethidium Bromide (AO/EB) Staining

Before inoculating coverslips with RAW264.7 macrophages suspensions, the coverslips were placed in 6-well plates. After division into control/LPS/paeoniflorin/Pae–PPNPs/Pae–PPNPs–DS groups, the cells were incubated for 24 h, resuspended in a 10-fold diluted buffer solution. Working solution (10 μL), prepared by combining AO/EB (E607308; Sangon Biotech Co. Ltd.) in a 1:1 ratio, was added to the cell suspension (90 μL) in the dark (10 min). Apoptosis was examined using a DM IL inverted microscope (Leica).

Cellular Uptake

Since activated macrophages overexpress SR-AI, an inflammatory cell model was constructed using LPS-activated RAW264.7 macrophages. Rhodamine B (S19124; Yuanye Biotechnology Co. Ltd.) was encapsulated in nanoparticles instead of paeoniflorin to explore nanoparticle uptake/distribution by RAW264.7 macrophages. The cells were then treated with rhodamine B-labelled nanoparticles and incubated for 2 h. Nuclei were stained with 4′,6-diamidino-2-phenylindole (DAPI) (C0060; Solarbio Science & Technology Co. Ltd). Cellular uptake was observed using an FV1000 laser scanning confocal microscope (Olympus).

Real-Time Quantitative Polymerase Chain Reaction (RT-qPCR)

RT-qPCR was used to study the mRNA expression of M1 and M2 macrophage markers. RAW264.7 cells (2×10^5) were inoculated into 24-well plates, which were divided into control/LPS/paeoniflorin/Pae–PPNPs/Pae–PPNPs–DS groups for post-treatment and culture for 24 h. The cells were harvested, and the total RNA was extracted with TRIzol reagent. The mRNA expressions of *iNOS, IL-6*, and *TNF-α* in M1 macrophages *and IL-10, Arg-1* and *TGF-β* in M2 macrophages were calculated via the $2^{-\Delta\Delta CT}$ method, and *GAPDH* was used as a reference gene. Primers used for RT-qPCR are listed in Table 1.

Table 1 Primer Sequences Used in RT-qPCR

Corresponding Gene Name	Primer Sequences
	F:5′-TGTGGATGGCCCCTCTGGAA-3′
GAPDH	
	R:5′-TGACCTTGCCCACAGCCTTG-3′
	F:5′-GAGACGCACAGGCAGAGG-3′
iNOS	
	R:5′-CAGGCACACGCAATGATGG-3′
	F:5′-CTGGAGCCCACCAAGAACGA-3′

(*Continued*)

https://doi.org/10.2147/IJN.S516434

Table 1 (Continued).

Corresponding Gene Name	Primer Sequences
IL-6	
	R:5′-GCCTCCGACTTGTGAAGTGGT-3′
	F:5′-AGGGTCTGGGCCATAGAACT-3′
TNF-α	
	R:5′-CCACCACGCTCTTCTGTCTAC-3′
	F:5′-CCAGTACAGCCGGGAAGACA-3′
IL-10	
	R:5′-GAAGGCAGTCCGCAGCTCTA-3′
	F:5′-TTGGGTGGATGCTCACACTG-3′
Arg-1	
	R:5′-GTACACGATGTCTTTGGCAGA-3′
	F:5′-GCCACTGCCCATCGTCTACT-3′
TGF-β	
	R:5′-CACTTGCAGGAGCGCACAAT-3′

Experimental Animals

Wild-type AB zebrafish (accession number: 2022120702) were raised in a centralized laboratory culture system. They spontaneously propagated in pairs, were maintained under a 12:12 (light: dark) photoperiod at 28°C (pH 7.4), and were fed live brine shrimp thrice daily.

Thirty healthy male Sprague–Dawley rats (6-weeks old, 165–210 g) (accession number: 2022101305) were procured from the Experimental Animal Center of Heilongjiang University of Chinese Medicine (animal certificate: SYXK [black] 2022-009). Rats were acclimated for 1 week prior to experimentation. All studies were approved by the Institutional Animal Care and Use Committee (IACUC) of Heilongjiang University of Chinese Medicine (accession number: 2022101305) and were conducted in accordance with the National Laboratory Animal Management Regulations and the principles of experimental animal protection.

Biocompatibility

The hemolysis rate is crucial for assessing drug safety and biocompatibility.[20] Erythrocyte concentration was reduced to 2% using normal saline and the mixture was incubated for 60 min at 37 °C. Paeoniflorin/Pae–PPNPs–DS were added to the diluted erythrocyte solution at 25/50/100 μg/mL. After a series of processing, the supernatant's optical density (OD) was quantified using an ultraviolet-visible spectrophotometer (WFZUV-4802H; Unicosh). Normal saline and 0.1% SDS were used as negative and positive controls, respectively.

$$Hemolysis(\%) = \frac{A_{sample} - A_{negtive\ control}}{A_{positive\ control} - A_{negtive\ control}} Ga€100\%$$

Acute Toxicity

Zebrafish are ideal models because their metabolism of traditional Chinese medicine in vivo is similar to that of humans.[21,22] Zebrafish larvae (3 d postfertilization) were randomly selected and maintained in 12-well plates with culture water containing Pae–PPNPs–DS (200/400/600/800/1000/1200/1400/1600/1800 μg/mL). The control group comprised zebrafish cultured in water. Observation windows were set at 8-h intervals. The number of larvae that died in each group was recorded to determine the mortality rate and compute the sublethal concentration (LC10) and lethal curves.

Animal Model Generation

Collagen-induced arthritis (CIA) is a classic RA animal model.[23] CIA was used to induce RA in rats. In brief, incomplete Freund's adjuvant (1 mL) (F5881; Sigma-Aldrich) was formulated with Bacillus Calmette-Guérin vaccine (10 mg) (R19021; Ruichu Biotechnology Co. Ltd.) to form complete Freund's adjuvant, which was emulsified with an equal volume of bovine type II collagen (2 mg/mL) (20022; NeoBioscience Technology Co. Ltd.) On day 0 (baseline), an emulsifier was injected into the tail roots of rats for the initial immunization, followed by boosters on days 3 and 7. Rats were divided into four groups of six: normal, CIA, Pae–PPNPs, and Pae–PPNPs–DS. Paeoniflorin/Pae–PPNPs/Pae–PPNPs–DS (10 mg/kg/day) were administered via tail vein injection. Rats were euthanized on day 39. Knee joint tissues were excised, and blood samples were collected.

Assessment of Toe Swelling and Arthritis in Rats

Photographs of the hind paws/swelling/AI were obtained at 7-d intervals after the model was established. Foot volume was measured using the drainage volume method.[24] The foot swelling rate reflected the severity of RA.

$$Toe\ swelling\ rate = \frac{(foot\ volume\ on\ day\ n\ after\ modelling - initial\ foot\ volume)}{initial\ foot\ volume} Ga€''100\%$$

The joint score method (hindfoot)[25] was used to evaluate RA: 0, normal joints with no swelling; 1, slightly swollen ankle/toe joint; 2, slight swelling from the ankle to the toe/metacarpal joint; 3, moderate swelling from the ankle to the toe/metacarpal joint; 4, erythema and severe swelling from the ankle joint to the sole. The joint swelling score was calculated as the sum of the two hindfoot scores, with a maximum score of eight and was referred to as the arthritis index (AI).

Body Mass and Spleen Index of Immune Organs

Body mass was quantified at 7-d intervals. The spleen index was used to assess the effect of Pae–PPNPs–DS on immune organs. The spleen index was calculated as follows:

$$Immune\ organ\ index = \frac{quality\ of\ immune\ organs}{body\ mass}$$

Liver and Renal Function Markers

At the end of treatment, the alanine aminotransferase (ALT), aspartate aminotransferase (AST), blood urea nitrogen (BUN), creatinine (Crea) (ml076531, ml092712, ml076478, M12C4B, Shanghai Enzyme-linked Biotechnology Co., Ltd.) levels were analyzed by the autoanalyzer device (AU5800, Beckman, Inc.).

Phenotypic Conversion Cytokine Assays

Enzyme-linked immunosorbent assays were used to quantify the concentrations of *TNF-α*/*IL-1β*/*IL-10*/*iNOS*/*Arg-1* (important markers of cell polarization and indicators of macrophage polarization).

Histological Analysis

After treatments, the ankle joints were stained with hematoxylin and eosin staining (C0105S; Biotime Biotechnology) and observed by a DM3000 optical microscope (Leica).

Western Blot

The treated macrophages were collected and proteins from macrophages were extracted on ice using RIPA lysate, and the protein content of the extracted proteins was determined using a bicinchoninic acid (BCA) kit. Sodium dodecyl sulfate-polyacrylamide gel (SDS-PAGE) electrophoresis was conducted by protein transfection and subsequent block in tris-buffered saline with Tween-20 buffer containing 5% defatted milk powder for 2 h. Polyvinylidene fluoride membranes were incubated with anti-p-*STAT1* (1:1000) primary antibody and anti-p-*STAT6* (1:1000) primary antibody for 12 h at 4°C, and then incubated with horseradish peroxidase (HRP)-coupled goat anti-rabbit IgG secondary antibody incubated for 2 h. The enhanced chemiluminescence kit was used to develop color, and the signal was detected by a chemiluminescence imaging analyzer.

After extracting protein from the synovial tissue of the rats, the protein was quantified using the BCA kit. Briefly, it was separated by SDS-PAGE electrophoresis and sealed by membrane transfer. Anti-p-*STAT1* (1:1000) primary antibody, anti-p-*STAT6* (1:1000) primary antibody and anti-*MMP-3* (1:1000) primary antibody were added and incubated overnight, and then the secondary antibody was added to continue the incubation. Imaging was performed using a chemiluminescence imager.

Immunofluorescent Staining

The joint samples of the CIA rats were stained with antibody against *CD68*/*iNOS*/*Arg-1* (1:100) (sc-20060 [Santa Cruz Biotechnology]/sc-7271 [Santa Cruz Biotechnology]/sc-271430 [Santa Cruz Biotechnology]). Goat anti-rabbit IgG H&L (ab6721, Abcam Plc) (1:400) antibody was incubated in the dark for 1 h at room temperature. The nucleus was stained with DAPI, and all sections were imaged using a laser scanning microscope to determine the polarity conversion of macrophages.

Statistical Analysis

Statistical analyses were performed using Microsoft Excel software and GraphPad Prism 8. A P value of <0.05 was considered to indicate statistical significance. Each assay had at least three replicates and was repeated three times independently. After confirming that the values followed a normal distribution, a two-tailed Student's t-test was applied to determine the significant differences. Data are expressed as mean±SD. Between-group differences were analyzed using one-way ANOVA.

Results

Nanoparticle Preparation

Nanoparticles exhibited a smaller particle size (112.5±1.3 nm) and good dispersion (PDI, 0.104±0.021) when the input of Batch 2 was 10 mg compared with that when other inputs were used (Batches 1–3) (Table 2). In Batch 5, the particle size distribution was narrow and stable. In Batches 7–10, the particle surface charge was adjusted by gradually adding DOTAP. With increasing DOTAP, the zeta potential shifted from negative (−1.86±0.38 mV) to positive (19.74±0.42 mV). Batch 9 was selected for further study based on the particle size and dispersibility criteria. In Batches 11–13, the electrostatic adsorption effect was observed to connect the DS. With gradually increasing DS input, the zeta potential decreased. The electrostatic adsorption effect increased in particle size. Based on the screening criteria, Batch 12 was determined to be the optimal input composition.

Content Determination

To determine specificity of the nanoparticles, the peaks were examined during the standard paeoniflorin the retention time of 7.537 min (Figure S1A). The HPLC diagram of the Pae–PPNPs–DS solution exhibited a stable peak shape and good peak separation in chromatographic peak resolution (Figure S1B). Peaks were absent in the negative standard solution during the paeoniflorin retention period (Figure S1C). In addition, the standard curve (Y=20779X-26038) (R^2=0.9992) for the

Table 2 Characterization of Different Nanoparticle Batches

Batch	Pae (mg)	PLGA:PCADK	DOTAP (mg)	DS (mg)	Size (nm)	PDI	Zeta (mV)
1	5	–	–	–	118.2±2.1	0.116±0.010	−6.73±0.24
2	10	–	–	–	112.5±1.3	0.104±0.021	−8.65±0.52
3	15	–	–	–	117.4±2.5	0.113±0.018	−7.18±0.37
4	10	2:3	–	–	124.8±1.6	0.227±0.084	−6.14±0.45
5	10	1:1	–	–	120.3±0.9	0.136±0.067	−7.52±0.18
6	10	3:2	–	–	121.7±1.5	0.175±0.036	−6.21±0.32
7	10	1:1	1	–	357.1±5.6	0.174±0.011	−1.86±0.38
8	10	1:1	2	–	167.5±2.4	0.214±0.009	10.12±0.43
9	10	1:1	3	–	135.9±0.9	0.207±0.013	14.68±0.27
10	10	1:1	4	–	159.6±0.6	0.119±0.027	19.74±0.42
11	10	1:1	3	0.5	198.1±4.6	0.382±0.076	−10.9±0.02
12	10	1:1	3	1	192.2±1.4	0.225±0.015	−16.3±0.26
13	10	1:1	3	1.5	257.5±9.7	0.308±0.019	−29.6±0.65

Notes: Data are expressed as mean±SD. "–" indicates that the material is added in the right amount.
Abbreviations: DOTAP, 1,2-dioleoyl-3-trimethylammonium propane; DS, dextran sulfate; PCADK, poly(cyclohexane-1,4-dimethylene ketal); PDI, polydispersity index; PLGA, poly(lactic-co-glycolic acid).

concentration (X) versus peak area (Y) of paeoniflorin is presented in Figure S2 demonstrating a robust linear correlation between paeoniflorin concentration and peak area with a quantitative lower limit of 1.0 μg/mL. To assess precision, the RSD of the paeoniflorin peak area was measured in reference solutions of low/medium/high mass concentrations and were found to be 0.63%/0.41%/0.53%, respectively. The RSD of the paeoniflorin mass concentration in Pae–PPNPs–DS was 1.31%, demonstrating repeatability of the nanoparticle analysis. The RSD of the paeoniflorin peak area was 1.26%, demonstrating stability. Further, the average spike recovery of paeoniflorin was 99.02% with an RSD of 1.15%.

Nanoparticle Characterization

The Pae–PPNPs–DS prepared using the optimal formula exhibited a milky-white color (Figure 2A). Transmission electron microscopy revealed that the Pae–PPNPs–DS were rounded, with aggregation and adsorption, and were spherical/elliptical (Figure 2B). The Pae–PPNPs–DS had a narrow particle size distribution (PDI, 0.225±0.015), an average particle size of 192.2±1.4 nm, and a zeta potential of −16.3±0.26 mV (Figure 2C and D). Compared with regular nanoparticles, polymer–lipid hybrid nanoparticles with surface modifications enhance drug targeting/EE/active delivery while increasing bioavailability/compatibility.[26,27] Pae–PPNPs–DS had an EE of 86.15±1.37% and a DL of 10.41±0.26%. The preparation process was reproducible. The prepared nanoparticles exhibited optimal physicochemical properties.

In vitro Stability

Particle size remained unchanged in PBS (25°C) (Figure 3A). Pae–PPNPs–DS exhibited no aggregation and excellent stability, rendering them suitable for further research. Nevertheless, in PBS containing 10% FBS (37°C), the particle size of Pae–PPNPs–DS increased at 24 h and 48 h.

In the two types of environmental simulation media, the surface potential of Pae–PPNPs–DS fluctuated within the range of −11 to −16 mV over 48 h (the absolute value of the zeta potential is displayed in Figure 3B). The overall potential exhibited minimal fluctuations. In contrast, the individual values demonstrated greater variability (Figure 3B). Pae–PPNPs–DS demonstrated good stability in in vitro and in vivo for 48 h.

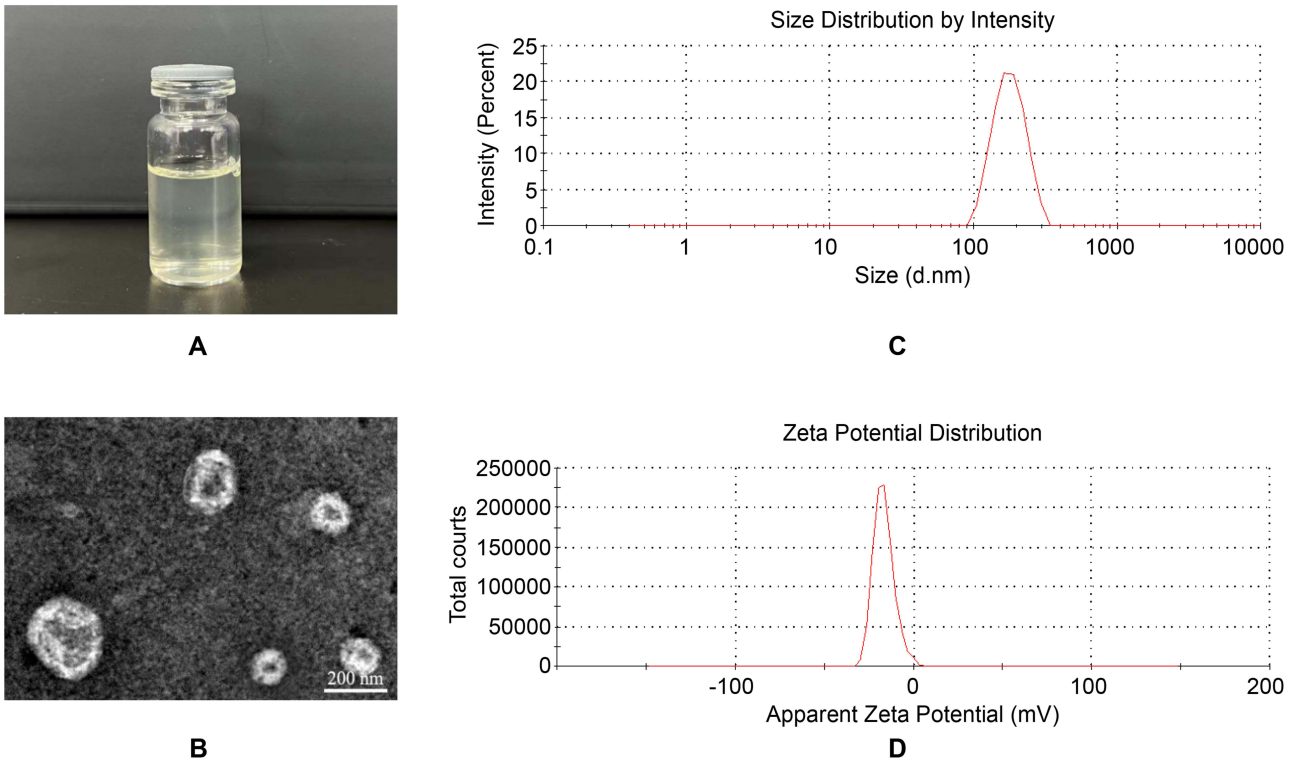

Figure 2 Photographic images (**A**), Transmission Electron Microscopy images (**B**), particle size distribution (**C**), and zeta potential (**D**) of the Pae–PPNPs–DS solution at a concentration of 1 mg/mL.

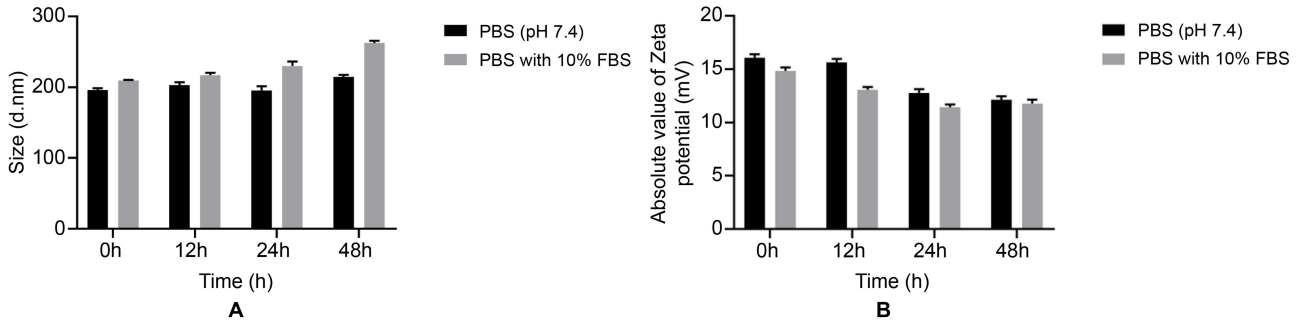

Figure 3 Variation in particle size (**A**) and absolute value of zeta potential (**B**) of Pae–PPNPs–DS in different media instability experiments. Data are presented as mean±SEM (n=3).
Abbreviations: FBS, fetal bovine serum; PBS, phosphate-buffered saline.

In vitro pH Sensitivity of Pae–PPNPs–DS

Pae–PPNPs–DS exhibited two distinct profiles: an initial and a sustained-release profile (Figure 4). During the initial 4 h, paeoniflorin was released abruptly at pH 5.0/7.4. Following the initial abrupt release, nanoparticles in media with different pH values entered the sustained-release stage. Nevertheless, the release rate of Pae–PPNPs–DS was faster at pH 5.0 than at pH 7.4. After 48 h of sustained release, the cumulative amount of paeoniflorin released from Pae–PPNPs–DS at pH 5.0 was higher than that at pH 7.4. Drug release from Pae–PPNPs–DS was pH-dependent, and all observed results were related to the pH-responsive properties of Pae–PPNPs–DS.

Pae–PPNPs–DS Enhances Macrophage Activity

Toxicity of blank/drug-loaded nanoparticles to RAW264.7 macrophages was measured using the MTT assay. Macrophage viability was equal between the PPNPs–DS-treated and control groups (Figure 5). Macrophage viability

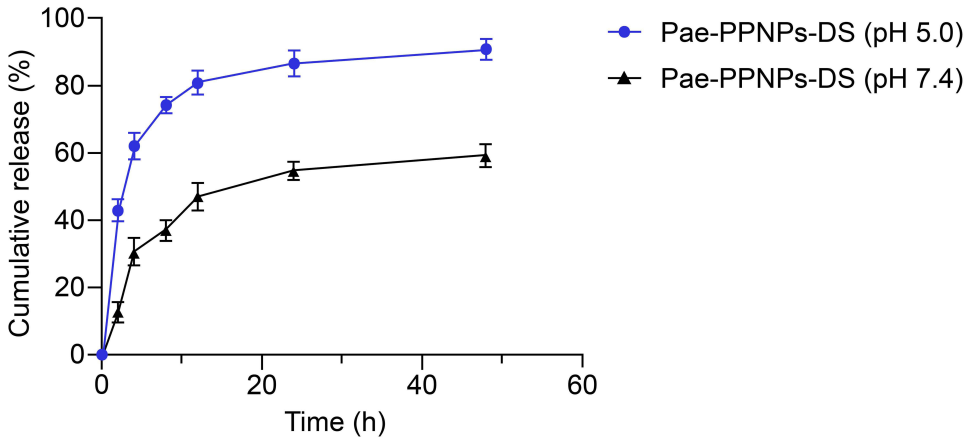

Figure 4 In vitro release profiles of Pae–PPNPs–DS in media at pH 5.0 and 7.4.

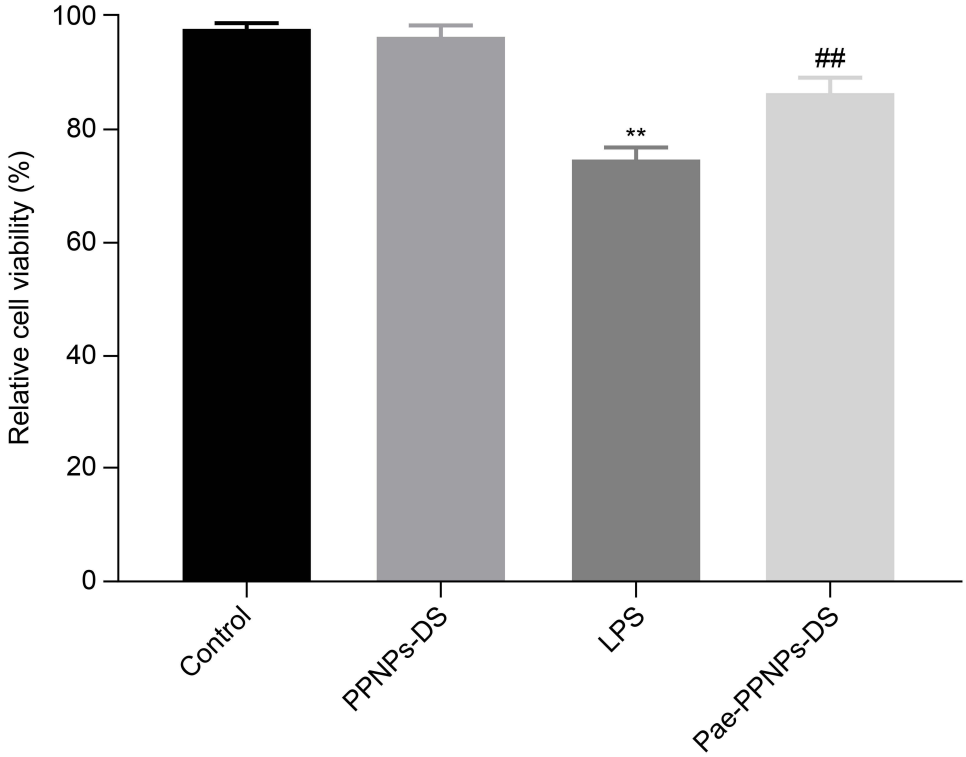

Figure 5 Effects of PPNPs–DS/Pae–PPNPs–DS on LPS-induced RAW264.7 cell viability. Data are presented as mean±SD (n=6). $^{**}P<0.01$ vs control; $^{\#\#}P<0.01$ vs LPS.
Abbreviation: LPS, lipopolysaccharide.

decreased following LPS treatment ($P<0.01$) but increased following Pae–PPNPs–DS treatment ($P<0.01$), indicating that LPS was toxic. Blank nanocarriers were not cytotoxic, while Pae–PPNPs–DS enhanced macrophage viability that had been compromised by LPS treatment.

Pae–PPNPs–DS Attenuates LPS-Induced Apoptosis of Macrophages

Apoptosis was higher in the LPS-induced group ($P<0.01$) than that in the control group. While apoptosis was reduced in all the administered groups, Pae–PPNPs–DS exhibited the least apoptosis (Figure 6A and B).

https://doi.org/10.2147/IJN.S516434

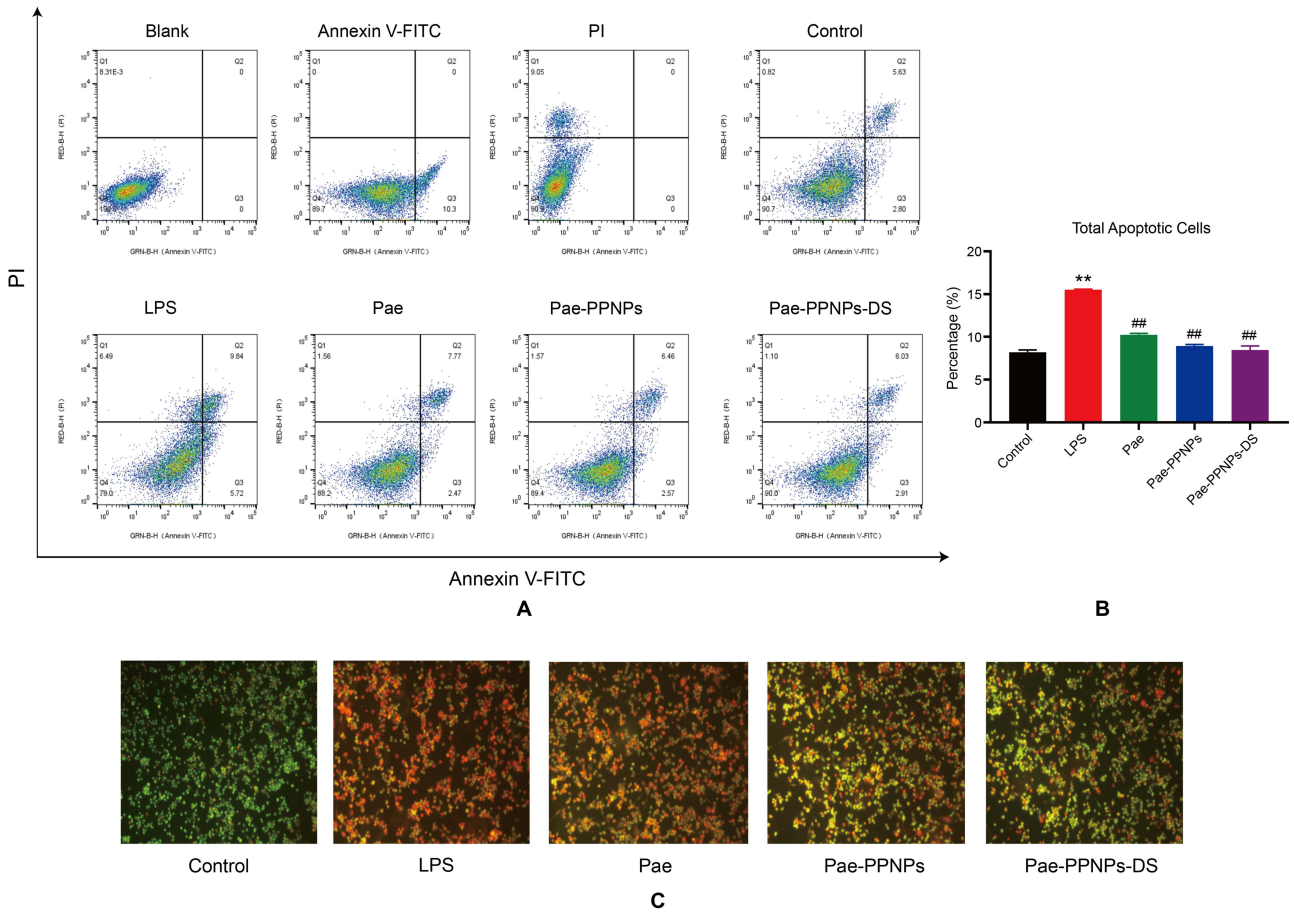

Figure 6 Flow cytometric detection of apoptosis (**A**), the mean percentage of apoptotic cells (**B**), and apoptosis after AO/EB staining (**C**) (scale bar, 200 μm). Data are presented as mean±SD (n=6). $^{**}P<0.01$ vs control; $^{\#\#}P<0.01$ vs LPS.

Control macrophages exhibited high-intensity green fluorescence with a low rate of apoptosis (Figure 6C). Conversely, LPS-induced macrophages had a higher apoptosis rate. Following paeoniflorin/Pae–PPNPs/Pae–PPNPs–DS administration, apoptosis was gradually decreased. Apoptosis in Pae–PPNPs–DS demonstrated observable attenuation.

Pae–PPNPs–DS Improves Macrophage Uptake Efficiency

Red fluorescence in normal macrophages was relatively low (Figure 7A and B), indicating the minimal uptake of rhodamine B. Fluorescence uptake of inflammatory macrophages was higher than that in normal macrophages, suggesting that macrophage phagocytosis may depend on activation. In activated RAW264.7 macrophages, PPNPs–DS uptake was higher than PPNPs ($p < 0.01$), with PPNPs–DS exhibiting good targeting properties.

Pae–PPNPs–DS Regulates Macrophage Polarization Through the STAT Signalling Pathway

STAT1 and *STAT6*, which are key players of the STAT signaling pathway, were detected based on the Western blot experiments, *STAT1* mediates the activation of the M1 macrophages and *STAT6* regulates the polarization of the M2 macrophages.[28] As shown in Figure 8A and B, p-*STAT1* expression was significantly up-regulated ($p < 0.01$) in normal macrophages after LPS treatment, and showed down-regulation of p-*STAT1* expression ($p < 0.01$) after exposure to Pae, Pae–PPNPs, and Pae–PPNPs–DS. The p-*STAT1* expression was lower in Pae–PPNPs–DS compared to Pae and Pae–PPNPs ($p < 0.01$). The expression of p-*STAT6* was additionally decreased after macrophage exposure to LPS ($p < 0.01$), and gradually increased after treatment with Pae, Pae–PPNPs, and Pae–PPNPs–DS ($p < 0.01$), with Pae–PPNPs–DS in particular showing better results ($p < 0.01$).

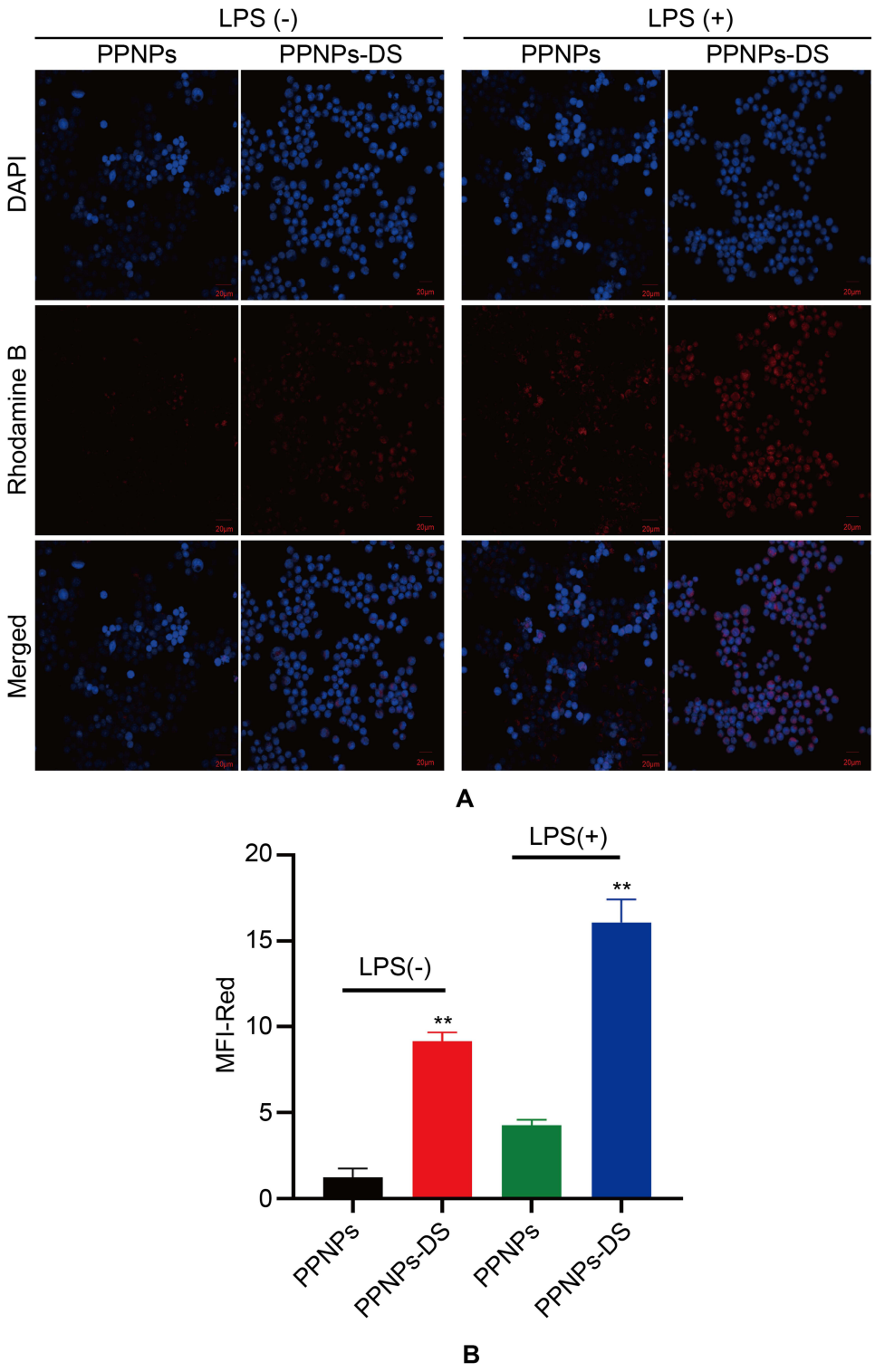

Figure 7 Cellular uptake of rhodamine B-labeled PPNPs/PPNPs–DS by RAW264.7 macrophages with/without (+/–) LPS-induced activation (**A**) (scale bar, 20 μm), RAW264.7 macrophage uptake fluorescence MFI value (**B**). Data are presented as mean±SD (n=3). $^{**}P<0.01$ vs PPNPs.
Abbreviations: DAPI, 4′,6-diamidino-2-phenylindole; PPNPs–DS, dextran sulfate-modified pH-responsive lipid–polymer hybrid nanoparticles.

https://doi.org/10.2147/IJN.S516434

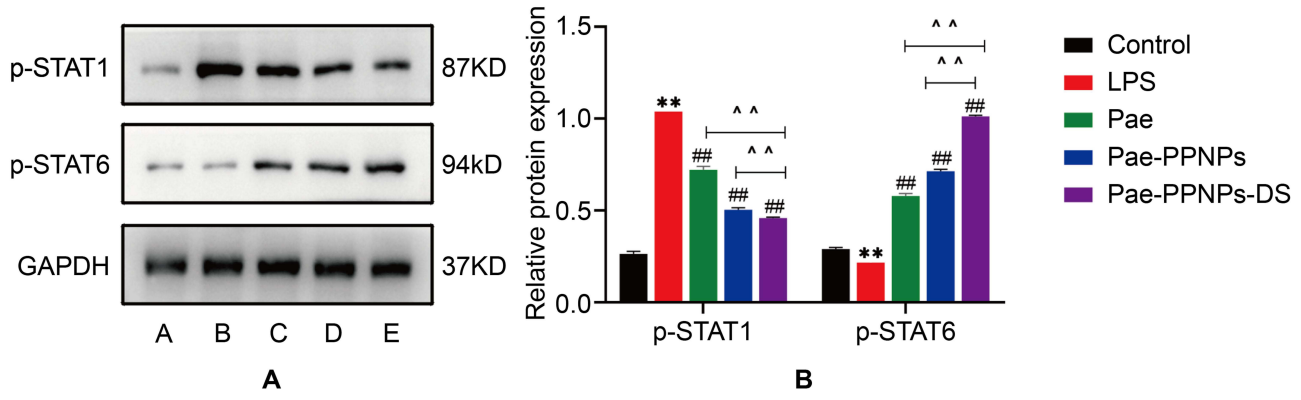

Figure 8 Protein trace images of p-*STAT1* and p-*STAT6* (**A**) and relative molecular expression (**B**). (A) Control group, (B) LPS group, (C) Pae group, (D) Pae–PPNPs group, (E) Pae–PPNPs–DS group. $^{**}P<0.01$ vs control group; $^{\#\#}P<0.01$ vs LPS group; $^{\wedge\wedge}P<0.01$ vs Pae–PPNPs–DS group.

Pae–PPNPs–DS Intervenes in the Expression of Macrophages Polarization Markers

qRT-PCR was used to determine the effects of Pae–PPNPs–DS on mRNA expression in RAW264.7 macrophages (Figure 9). The results showed that, compared with that observed in the control group, LPS-stimulated significantly increased mRNA expression of M1 phenotype-related markers in macrophages such as *iNOS, IL-6*, and *TNF-α*, while mRNA expression of *Arg-1, TGF-β*, and *IL-10* of M2 phenotype-related markers were decreased. LPS significantly promoted M1 polarization and inhibited M2 polarization. However, the Pae–PPNPs–DS group had significantly reduced mRNA expression of M1 phenotype markers and significantly enhanced the mRNA expression of M2 phenotype markers.

Pae–PPNPs–DS Exhibit High Biological Safety and Low Toxicity

Hemolysis tests demonstrated the safety of intravenous injection of paeoniflorin/Pae–PPNPs–DS. Hemolysis rates were <5% within the concentration range of 25–100 μg/mL (Figure 10A and B). Thus, paeoniflorin/Pae–PPNPs–DS exhibited good biocompatibility for in vivo use.

Following a 24-h acute toxicity test (Figure 11A), zebrafish larvae treated with 800 μg/mL Pae–PPNPs–DS exhibited signs of mortality. No zebrafish death was observed in the experimental/control groups at this concentration. A dose-toxicity curve showed that the LC10 of Pae–PPNPs–DS was 834.57 μg/mL (Figure 11B).

Pae–PPNPs–DS Relieves RA-Related Symptoms

The CIA rats were used as a model to assess the therapeutic effects of paeoniflorin/Pae–PPNPs/Pae–PPNPs–DS in vivo (Figure 12A). Seven days after the CIA model was established, toe swelling and the AI reached their highest levels in the CIA and administration groups. After 28 days of treatment, there was an increase in foot/paw swelling in CIA rats compared with that in controls ($P<0.01$). The degree of foot swelling in CIA rats was reduced to varying degrees by paeoniflorin/Pae–PPNPs/Pae–PPNPs–DS. Pae–PPNPs–DS exhibited the most significant effect, with an average reduction of 40.44% (Figure 12B). The AI of CIA rats was higher than that of control rats ($P<0.01$). Paeoniflorin/Pae–PPNPs/Pae–PPNPs–DS exhibited disparate and sustained declining trends throughout the treatment period. After the treatment period, Pae–PPNPs–DS exhibited the most pronounced decline ($P<0.01$). The mean AI score was 1.90, indicating that the trend in AI scores matched the degree of foot swelling (Figure 12C). Macroscopic observation of the hind paw revealed severe foot/paw swelling and loss of paw function in CIA rats compared with that in controls (Figure 12D). Swelling was reduced in the paeoniflorin group; however, treatment outcomes were poor. Toe swelling of rats in the Pae–PPNPs/Pae–PPNPs–DS groups improved, with the Pae–PPNPs–DS group demonstrating the most notable improvement. The Pae–PPNPs–DS group exhibited a significant reduction in swelling, accompanied by restoration of paw function.

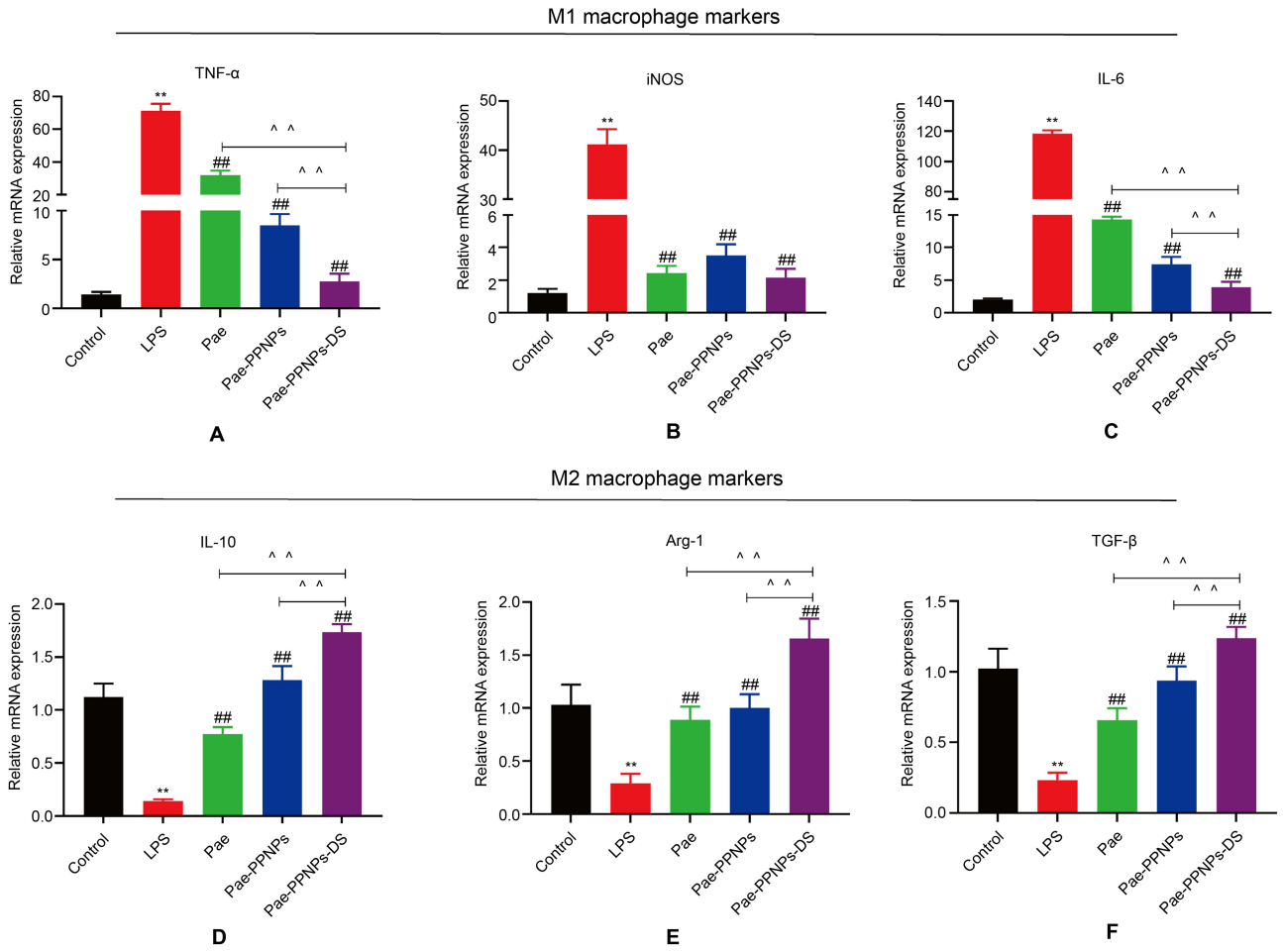

Figure 9 The relative mRNA expressions of macrophage M1 and M2 markers in RAW264.7 cells under different administration groups were analyzed by qRT-PCR. M1 markers: *TNF-α* (**A**), *iNOS* (**B**), *IL-6* (**C**); M2 markers: *IL-10* (**D**), *Arg-1* (**E**), *TGF-β* (**F**). Data are presented as mean±SD (n=6). $^{**}P<0.01$ vs control; $^{\#\#}P<0.01$ vs LPS; $^{\wedge\wedge}P<0.01$ vs Pae–PPNPs–DS.

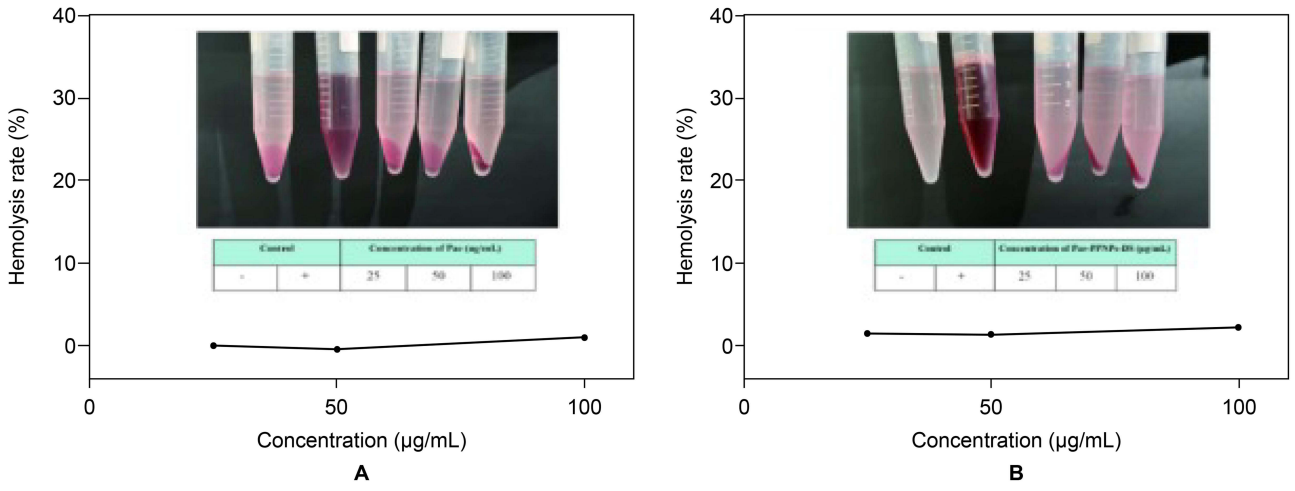

Figure 10 Hemolysis of paeoniflorin (**A**) and Pae–PPNPs–DS (**B**).

https://doi.org/10.2147/IJN.S516434

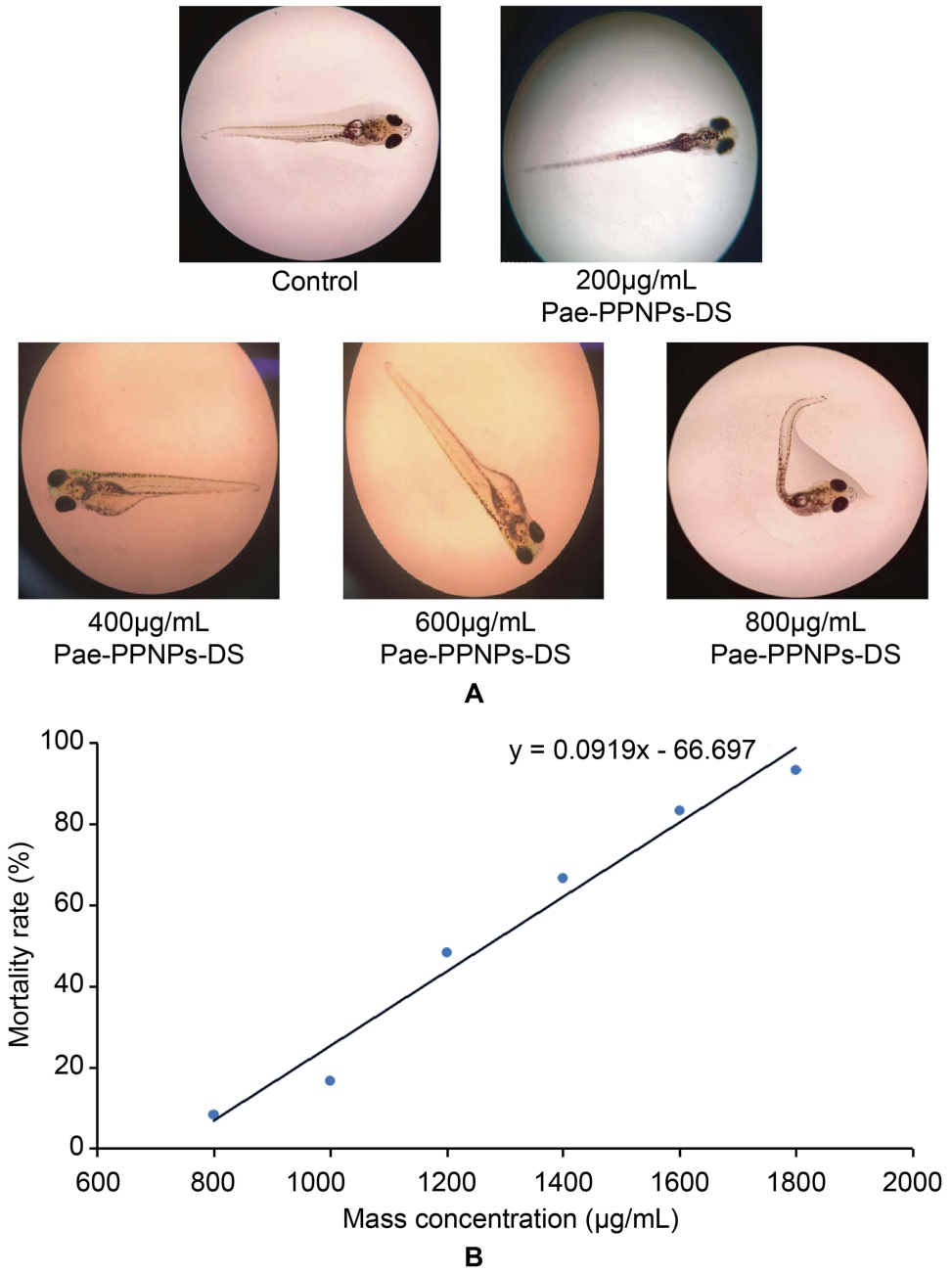

Figure 11 Microscopic images of zebrafish larvae in different concentrations of Pae–PPNPs–DS (**A**) and "mortality–concentration" effect curves (**B**).

Pae–PPNPs–DS Influence Body Weight and Splenic Index in CIA Rats

Body weight was positively correlated with time (Figure 13A), with a precise trend and no aberrant fluctuations indicating that the administration of the drugs did not result in sudden weight changes in experimental animals due to adverse reactions.

The CIA model increases spleen weight by exacerbating splenic damage and stimulating immune cell proliferation. The CIA group's splenic index was higher than that of the control group ($P<0.01$; Figure 13B). Compared with the CIA group, the paeoniflorin and Pae–PPNPs groups exhibited reduced spleen injury ($P<0.01$). Rats in the Pae–PPNPs–DS group exhibited a lower degree of splenic injury ($P<0.01$), suggesting that Pae–PPNPs–DS prevented RA-associated spleen injury and was immunosuppressive.

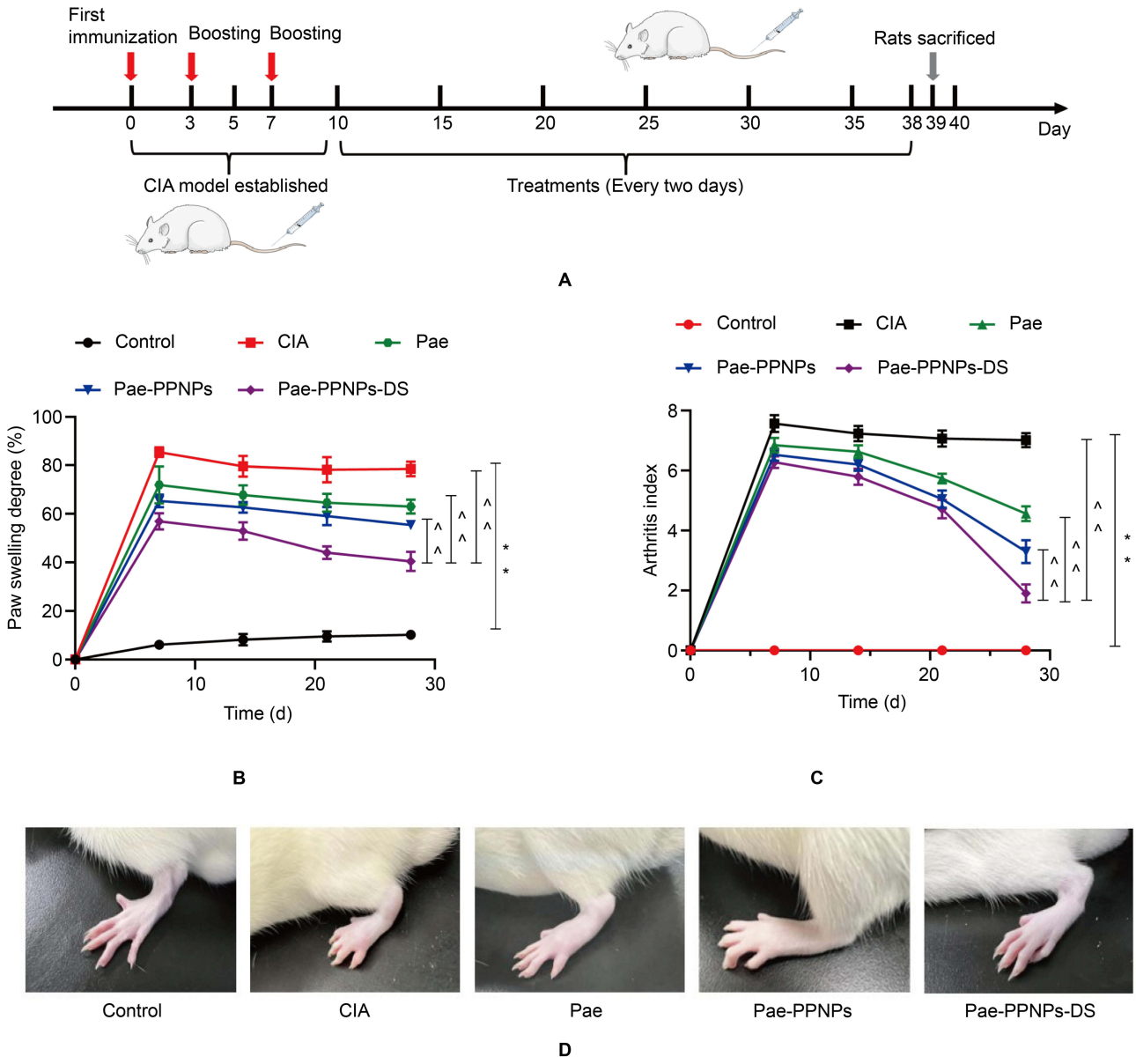

Figure 12 Effects of paeoniflorin/Pae–PPNPs/Pae–PPNPs–DS on the severity of arthritis in rats. Schematic diagram of CIA rat model establishment and therapeutic treatment (**A**), degree of foot swelling (**B**), arthritis index (**C**), and paw images showing foot swelling (**D**). Data are presented as mean±SD (n=6). ***P*<0.01 vs control; ^^*P*<0.01 vs Pae–PPNPs–DS.

Abbreviation: CIA, collagen-induced arthritis.

The analysis results of liver and kidney function markers showed that compared with that in the normal control, the levels of AST, ALT, BUN, and Crea in CIA group were significantly increased ($P<0.01$). Remarkably, these parameters were significantly decreased in Pae–PPNPs–DS group ($P<0.01$; Figure 13C–F), which may be attributed to the antioxidant and renal protective effects of Pae.

Pae–PPNPs–DS Modulate Macrophage Polarization Markers in CIA Rats

The expression levels of various cytokines were altered following the establishment of the CIA model ($P<0.01$; Figure 14A–E). Following paeoniflorin/Pae–PPNPs/Pae–PPNPs–DS administration, there was a decline in *TNF-α*/*IL-1β*/*iNOS* concentrations, accompanied by an increase in *IL-10*/*Arg-1* expression ($P<0.01$). Pae–PPNPs–DS induced more pronounced cytokine secretion changes than the other treatments ($P<0.01$). According to the experimental findings, Pae–

https://doi.org/10.2147/IJN.S516434

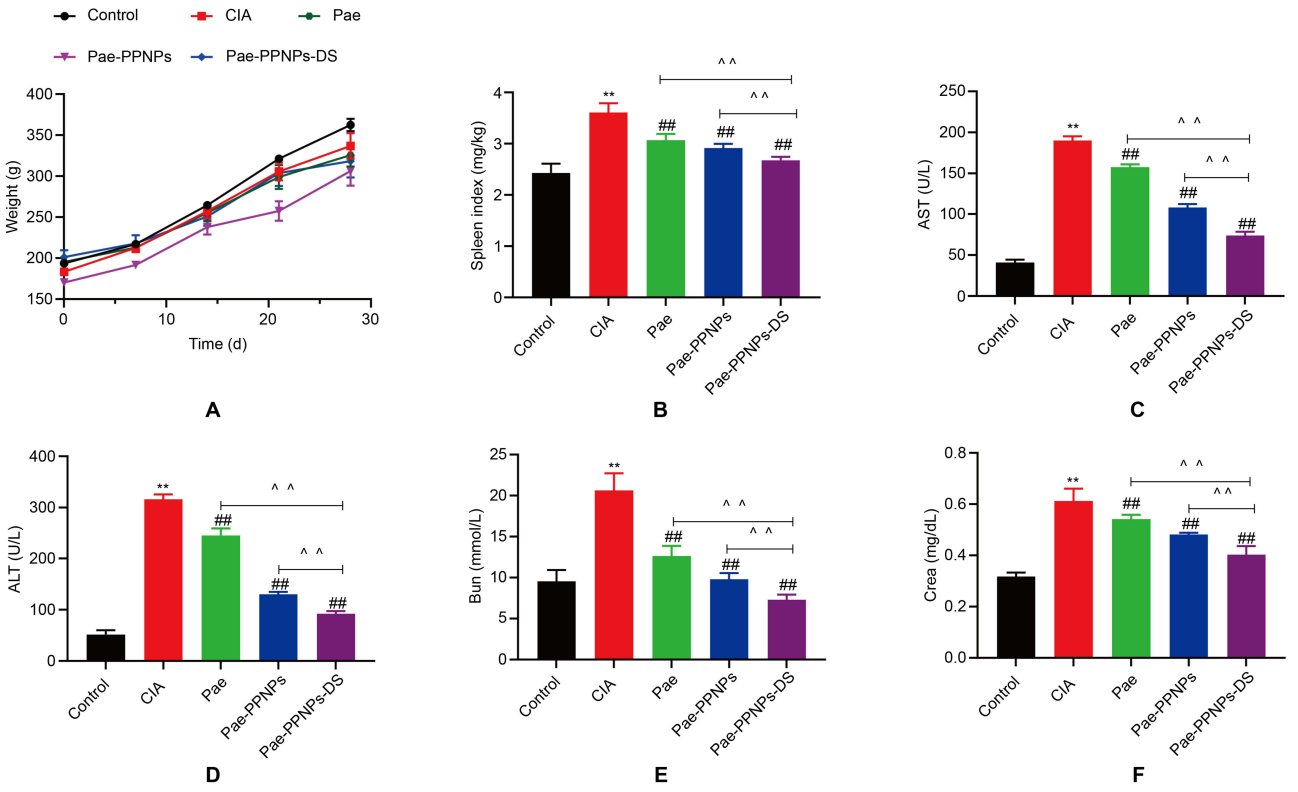

Figure 13 Effects of paeoniflorin/Pae–PPNPs/Pae–PPNPs–DS on body mass (**A**), splenic index (**B**), AST (**C**), ALT (**D**), BUN (**E**), and Crea (**F**) levels in rats. Data are presented as mean±SD (n=6). $^{**}P<0.01$ vs control; $^{\#\#}P<0.01$ vs CIA; $^{\wedge\wedge}P<0.01$ vs Pae–PPNPs–DS.

PPNPs–DS has the potential to lessen joint inflammation by reducing the production of pro-inflammatory M1 markers while promoting the production of anti-inflammatory M2 markers.

Pae–PPNPs–DS Alleviate Joint Destruction in CIA Rats

Histopathological examination of the ankle joint (Figure 15) revealed that the control group exhibited distinct tissue layers, smooth articular cartilage surfaces, normal chondrocyte morphology and structure, and normal synovial tissue without apparent inflammation. However, the CIA group had a disrupted articular cartilage surface and thickened synovial tissue, with connective tissue proliferation and lymphocyte infiltration. In the paeoniflorin group, the articular cartilage surface was rough, chondrocytes were disordered, and inflammatory cell infiltration occurred in certain areas. Rats in the Pae–PPNPs/Pae–PPNPs–DS groups exhibited a notable reduction in articular chondrocyte destruction and inflammatory cell infiltration. The Pae–PPNPs–DS group's articular chondrocyte interface was smooth with a normal synovium and few observable inflammatory cells, indicating that Pae–PPNPs–DS alleviated joint inflammation and synovial/connective tissue proliferation.

Pae–PPNPs–DS Regulates Transcription Factors and Cartilage Degrading Enzymes in CIA Rats

We further investigated the expression of transcription factors *STAT1*, *STAT6*, and cartilage degrading protease *MMP-3* in CIA rats. p-*STAT1* and *MMP-3* expression was significantly increased and p-*STAT6* expression was significantly decreased in CIA rats ($p < 0.01$) (Figure 16A and B). p-*STAT1* and *MMP-3* expression was significantly decreased and p-*STAT6* expression was significantly increased after Pae–PPNPs–DS treatment ($p < 0.01$).

Pae–PPNPs–DS Manipulate Phenotypic Polarization of Macrophages

CD68/*iNOS* was recorded a large amount of fluorescence intensity in CIA rats (Figure 17), indicating that their expression levels were increased. *Arg-1* exhibited a negative response, suggesting its expression was suppressed. In

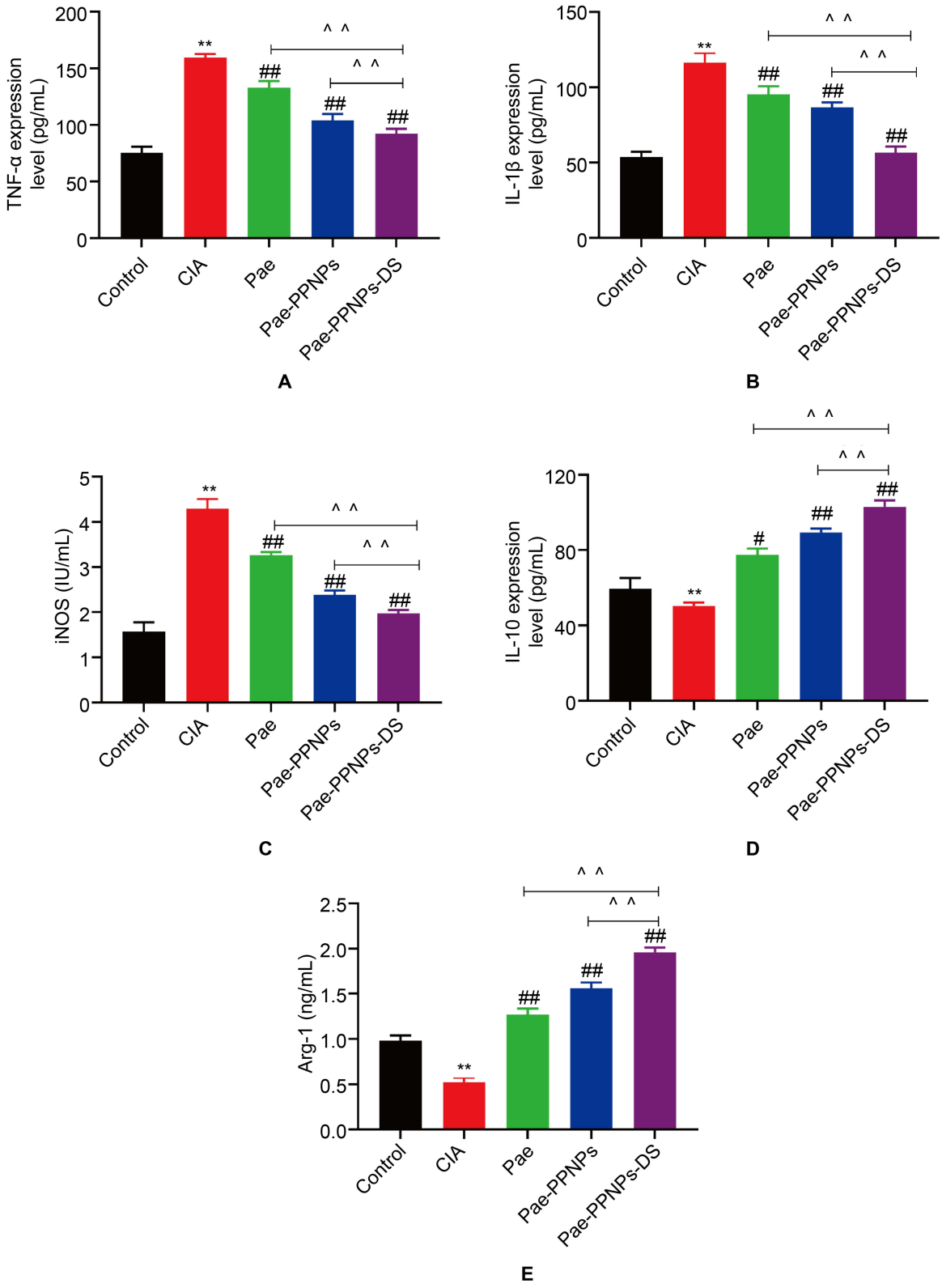

Figure 14 Effect of Pae–PPNPs–DS on serum *TNF-α* (**A**), *IL-1β* (**B**), *iNOS* (**C**), *IL-10* (**D**) and *Arg-1* (**E**) levels in CIA rats. Data are presented as mean ± SD (n = 6). ***P*<0.01 vs control group; $^{\#}p < 0.05$, $^{\#\#}P$<0.01 vs CIA group; $^{\wedge\wedge}P$<0.01 vs Pae–PPNPs–DS group.

https://doi.org/10.2147/IJN.S516434

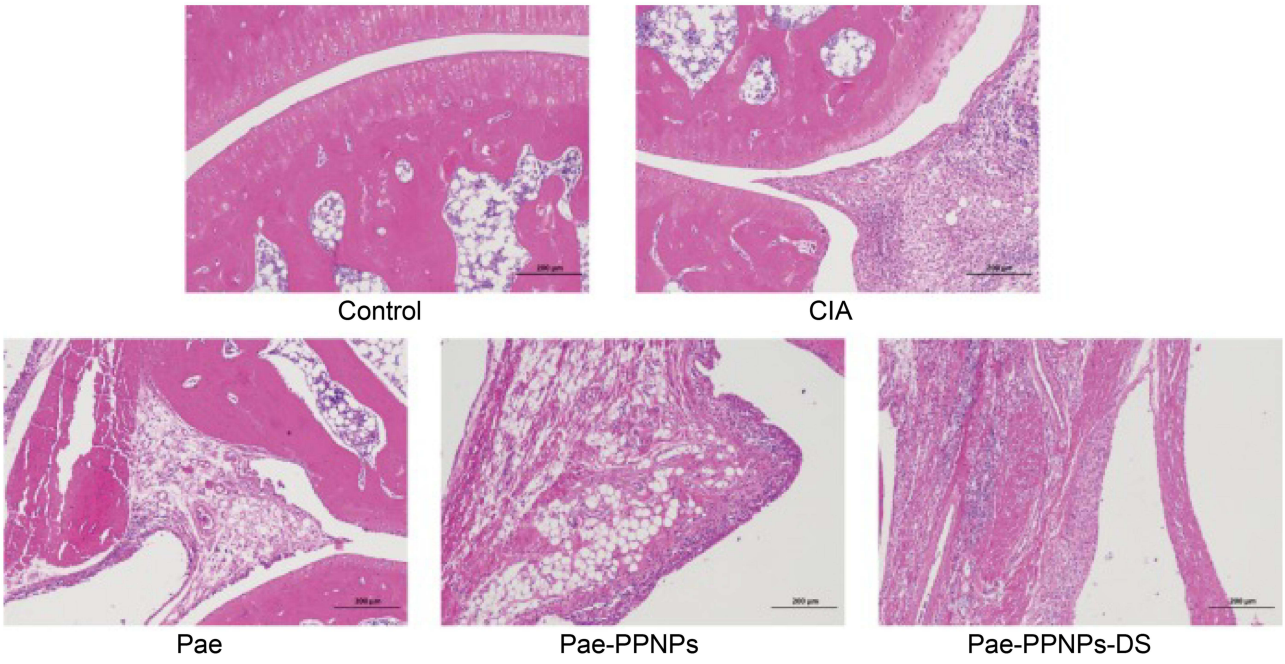

Figure 15 Pae–PPNPs–DS effect on ankle joint histopathology in CIA rats (scale bar, 200 μm).
Abbreviation: CIA, collagen-induced arthritis.

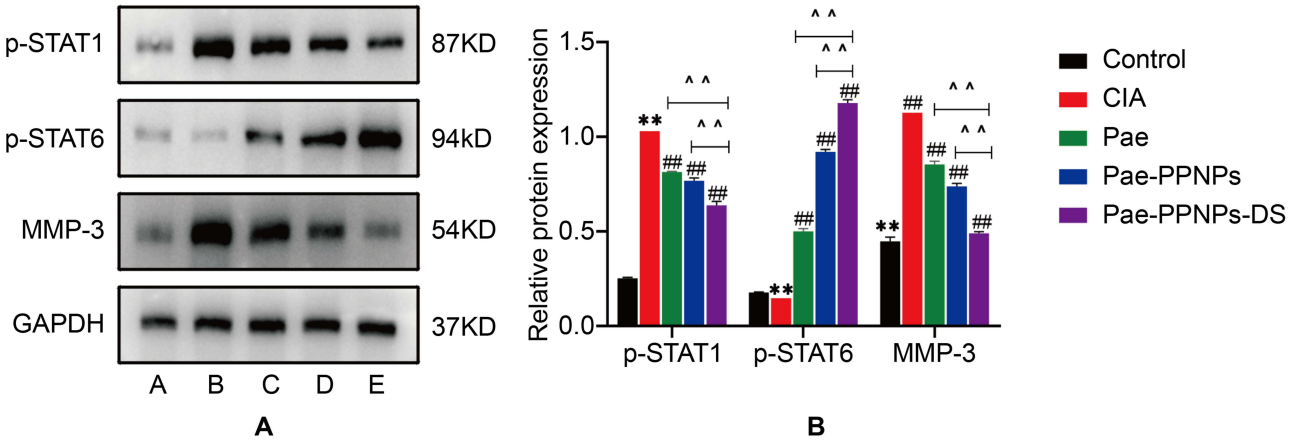

Figure 16 Protein trace image (**A**) and relative protein expression (**B**) of p-*STAT1*, p-*STAT6* and *MMP-3* in different groups. (A) Control, (B) CIA, (C) Pae, (D) Pae–PPNPs, (E) Pae–PPNPs–DS group. $^{**}P<0.01$ vs control group; $^{\#\#}P<0.01$ vs CIA group; $^{\wedge\wedge}P<0.01$ vs Pae–PPNPs–DS group.

subsequent administration groups, *CD68*/*iNOS* showed different degrees of reduction, and the expression of *Arg-1* was increased. The dominant macrophage polarization effect was observed in the Pae–PPNPs–DS group, suggesting that Pae–PPNPs–DS can promote the polarization of M1 macrophages into M2 macrophages to a greater extent than paeoniflorin/Pae–PPNPs by actively targeting macrophages.

Discussion

In this study, we developed Pae–PPNPs–DS, a nanodrug delivery system with therapeutic potential for RA that controls activated macrophage polarization and enhances mitochondrial activity. In the content determination, the specificity analysis indicated that the components of the carrier materials did not impede paeoniflorin detection, suggesting that this

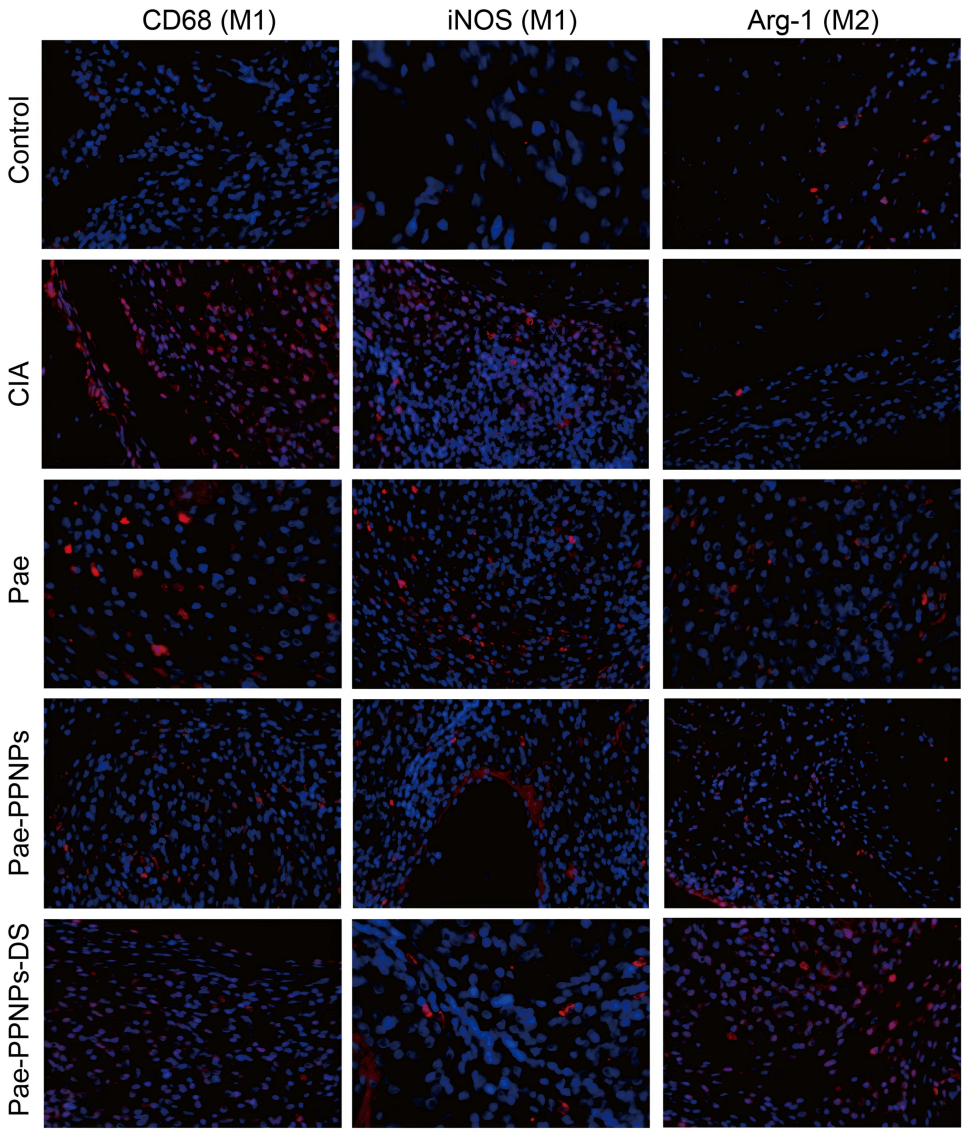

Figure 17 Immunofluorescence of rat joint tissues (scale bar, 100 μm).

technique can detect paeoniflorin. Further, the precision, repeatability, and stability analyses met the in vitro analysis standards. Meanwhile, the method exhibited satisfactory recovery of the spiked samples and was suitable for accurately analyzing biological samples. The results of the in vitro stability analysis showed that the particle size of the nanocarriers increased in the in vivo environment-simulating medium, and this phenomenon could be attributed to the formation of a protein crown on the nanocarrier's surface following contact with serum. This protein crown is easily recognized by cells/tissues, leading to an increase in particle size. The variation observed in the respective potentials of the two mimetic media might be attributed to the electrostatic adsorption of DS onto the nanoparticles, resulting in a small degree of detachment. The abrupt release of paeoniflorin in in vitro release experiments may be attributed to the acid-sensitive material, PCADK, which is present in nanoparticles, achieving enhanced dissolution and release of the encapsulated drug under acidic conditions, resulting in nanoparticles with pH-responsive drug release properties. Therefore, the above two experimental results show that Pae–PPNPs–DS released drugs continuously and achieved excellent stability for 48 h. The pH-responsive characteristics of Pae–PPNPs–DS, achieved under acidic conditions, accelerated drug release, resulting in the accumulation of the drug at sites of inflammation. Drug reservoirs form in vivo, which are beneficial for the treatment of RA. Pae–PPNPs–DS proved to be safe as a carrier formulation as shown by the immune index and liver and kidney

https://doi.org/10.2147/IJN.S516434

function results. The liver, kidney, and immune function of CIA arthritis rats were changed. After treatment, the liver, kidney, and immune function parameters of Pae–PPNPs–DS group significantly decreased ($P<0.01$). In a Western Blot assay, Pae–PPNPs–DS mediated macrophage polarization to attenuate inflammation via the STAT pathway. The superior performance of Pae–PPNPs–DS compared with that of a single paeoniflorin also suggests that it may play its own role in reducing inflammation as well as protecting liver and kidney function. In a biocompatibility experiment, Pae–PPNPs–DS also demonstrated good biocompatibility, providing the foundation for ensuing in vivo experiments.

Activated M1 macrophages inhibit mitochondrial oxidative phosphorylation and block the polarization of M1 macrophages to M2 macrophages. However, increased mitochondrial function improves metabolism and the repolarization of M2 macrophages.[29] Cytotoxicity experiments demonstrated that blank nanoparticles did not have a detrimental effect on the macrophage activity. However, macrophage activity diminished following LPS activation, while the administration of Pae–PPNPs–DS promoted cell viability. Because the MTT assay determined macrophage activity, including restoration of mitochondrial function levels, the therapeutic restoration of mitochondrial function by Pae–PPNPs–DS was hypothesized to improve the rephenotyping of M1 macrophages into M2 macrophages, thereby enhancing their anti-inflammatory activity. In the apoptosis experiment, while a low apoptotic rate was observed in normal macrophages, the apoptotic rate increased with LPS activation, consistent with previous findings.[30] Conversely, Pae–PPNPs–DS reduced inflammation by inhibiting macrophage apoptosis, suggesting that nanoparticles targeted inflammatory macrophages to improve drug efficacy. The targeted impact of Pae–PPNPs–DS further augmented macrophage polarization. LPS induces macrophage apoptosis through the caspase-dependent mitochondrial death pathway, reducing membrane potential and promoting the activation of caspase-3/9. Pae–PPNPs–DS may reduce macrophage activation by LPS by inhibiting caspase-dependent apoptosis of the mitochondrial death pathway.

Macrophages are innate immune cells that perform various functions in the immune system. We confirmed the active targeting of Pae–PPNPs–DS on macrophages using a cellular uptake assay. The activation of LPS-induced macrophages enhanced their phagocytic capacity. PPNPs–DS uptake by LPS-activated macrophages was higher than that by PPNPs. This was attributed to the high-affinity binding of DS-coupled nanoparticles to SR-AI on the surface of macrophages. DS promoted the targeted uptake of PPNPs–DS by RAW264.7 macrophages through SR-AI-mediated endocytosis. Following phagocytosis by macrophages, Pae–PPNPs–DS released drugs into acidic endosomes. Therefore, Pae–PPNPs–DS would require stabilization in a normal physiological environment and drug release in an acidic environment. PCADK, an acid-sensitive material, facilitates the anticipated arrival of nanoparticles in the acidic milieu of joint inflammation, where they are released via SR-AI-mediated endocytosis, demonstrating the pH-responsive performance of Pae–PPNPs–DS. Pae–PPNPs–DS exhibit active macrophage targeting and pH sensitivity.

Macrophages are subject to the action of transcription factors, such as STAT; *STAT1* and *STAT6* are important transcription factors in the JAK-STAT signaling pathway that is critical for macrophage polarization status. p-*STAT1* has been shown to consistently mediate inflammatory factor production in LPS-activated macrophages, whereas *STAT6* promotes M2 polarization.[31] In in vitro experiments, we examined the expression of p-*STAT1* and p-STAT6. p-*STAT1* protein expression was significantly decreased and p-*STAT6* protein expression increased after Pae–PPNPs–DS administration. The experiments confirmed the basis of the reversible process of M1 polarization by Pae–PPNPs–DS through p-*STAT1*, the activation of p-*STAT6* promotes M2 polarization, and the regulation of macrophage polarization by Pae–PPNPs–DS is associated with p-*STAT1* and p-*STAT6* is closely related. As activated macrophages affect inflammation by secreting pro-inflammatory factors and inhibiting anti-inflammatory factors, cytokine levels reflect the severity of joint inflammation. Paeoniflorin demonstrates anti-inflammatory properties, inhibiting the polarization of M1 macrophages and the expression of their inflammatory factors.[32–34] *TNF-α*/*IL-1β* play pivotal roles in immunity. *TNF-α*, the earliest mediator of inflammatory responses, activates T cells and other inflammatory factors.[35] *IL-1β* plays a role in acute protein synthesis and T cell activation.[36] *TNF-α*/*IL-1β* are important pro-inflammatory factors secreted by LPS-activated macrophages and *TNF-α*/*IL-1β*/*CD68*/*iNOS*/*IL-6* are markers of M1 macrophages. *IL-10* exerts immunomodulatory/anti-inflammatory effects and inhibits the expression of various cytokines, including *TNF-α*/*IL-1β*. In addition, *IL-10*/*Arg-1*/*TGF-β* serve as markers of M2 macrophages.

In qRT-PCR experiments, Pae–PPNPs–DS markedly inhibited LPS-induced M1 macrophage polarization and mRNA expression of its markers *iNOS, IL-6*, and *TNF-α*, and enhanced M2 macrophage polarization and the production of M2-

associated markers mRNA expression, including *Arg-1, TGF-β*, and *IL-10*. ELISA assays and immunofluorescence experiments further confirmed that paeoniflorin/Pae–PPNPs/Pae–PPNPs–DS decrease elevated *TNF-α*/*IL-1β* /*iNOS* levels and increase *IL-10*/*Arg-1* expression. Pae–PPNPs–DS have a greater impact on macrophage markers and macrophage factor expression than Pae–PPNPs, suggesting that Pae–PPNPs–DS regulate RA development by inhibiting the expression of M1 markers and inflammatory factors, promoting the expression of M2 markers and anti-inflammatory factors, and modulating M1/M2 phenotypic polarization. This is a process initiated by actively targeting macrophages, which could alleviate joint inflammation by reversing the pro-inflammatory to anti-inflammatory effects through modulation of cytokine expression, making it a promising strategy for treating RA.

In vivo pharmacodynamics experiments were conducted to confirm the effects of Pae–PPNPs–DS on RA. Compared to paeoniflorin/Pae–PPNPs, Pae–PPNPs–DS reduced joint swelling and AI scores in CIA rats. Pae–PPNPs–DS inhibited the expression of the pro-inflammatory factors, *TNF-α*/*IL-1β*, while increasing the secretion of the anti-inflammatory factor, *IL-10*. Compared to paeoniflorin/Pae–PPNPs, Pae–PPNPs–DS reduced joint inflammation/connective tissue proliferation and promoted synovial tissue repair. The improvement in joint symptoms may be attributed to paeoniflorin release by Pae–PPNPs–DS in an acidic microenvironment, which modulates drug efficacy. The favorable therapeutic effect may be attributed to the cladding action of nanoparticles, and the ELVIS (extravasation through leaky vasculature and the subsequent inflammatory cell–mediated sequestration) effect, which protects the structural integrity and biological activity of paeoniflorin, enhancing its efficacy. Nevertheless, the ELVIS effect results in leaky nanoparticle aggregation through neovascularization in inflamed joints and their uptake by inflammatory cells, indicating that Pae–PPNPs–DS has the potential to treat RA.[37] *MMP-3* is the most important protease leading to the degradation of shutdown cartilage.[38] p-*STAT1* and *MMP-3* expression was reduced and p-*STAT6* expression was elevated in CIA rats following Pae–PPNPs–DS administration. It suggests that Pae–PPNPs–DS attenuates joint inflammation by mediating the regulation of macrophage polarization by the transcription factors p-*STAT1* and p-*STAT6*, while reducing the expression of *MMP-3* to alleviate cartilage degradation in RA. As demonstrated by immunohistochemistry, Pae–PPNPs–DS inhibited the secretion of M1 macrophage markers, *CD68*/*iNOS*, and promoted *Arg-1* production confirming that Pae–PPNPs–DS can more accurately regulate macrophage polarization and induce a greater number of macrophages to polarize from the M1 to the M2 phenotype. These results indicated that macrophages undergo a phenotypic shift from M1 to M2 macrophages, further supporting the conclusion that Pae–PPNPs–DS regulate M1/M2 phenotypic polarization to control RA development.

This study has some limitations, which warrant further investigation. Although the nanoparticles developed in this study demonstrated therapeutic potential for RA, the synthesis scalability of lipid-polymer hybrid nanoparticles remains constrained by batch-to-batch variability and cost limitations, while the risks associated with their long-term in vivo biodistribution and metabolism warrant further investigation, potentially involving prolonged retention by the RES and cardiotoxicity from lipid degradation byproducts, along with regulatory complexities due to the absence of compendial methods. To bridge these gaps, on the basis of existing studies, we will expand the pharmacokinetics and signaling pathway mechanism of Pae–PPNPs–DS to verify the generalizability of our study. Future studies should focus on the drug metabolism process in vivo and accurately elucidate the relevant pathways and optimize the clinical therapeutic potential of Pae–PPNPs–DS through robust preclinical experiments.

Conclusion

This study findings indicate that Pae–PPNPs–DS have therapeutic benefits in RA. Pae–PPNPs–DS actively regulate phenotypic polarization and enhance intracellular mitochondrial viability in macrophages. Using Pae–PPNPs–DS to target and modulate macrophage polarization may be a promising therapeutic strategy to alleviate RA.

Abbreviations

SR-AI, Scavenger Receptor Class AI; DS, Dextran Sulfate; Pae, Paeoniflorin; PPNPs, Peptide-Polymer Nanoparticles; PCADK, Poly(ε-caprolactone)-b-poly(ethylene glycol)-b-poly(α,β-aspartic acid); PLGA, Poly(lactic-co-glycolic acid); DOTAP, 1,2-dioleoyl-3-trimethylammonium-propane; PDI, Polydispersity Index; RSD, Relative Standard Deviation; HPLC, High-Performance Liquid Chromatography; FBS, Fetal Bovine Serum; MTT, 3-(4,5-dimethylthiazol-2-yl)-

2,5-diphenyl tetrazolium bromide; LPS, Lipopolysaccharide; NO, Nitric Oxide; CIA, Collagen-Induced Arthritis; AI, Arthritis Index; *TNF-α*, Tumor Necrosis Factor Alpha; *IL-1β*, Interleukin-1 Beta; *IL-10*, Interleukin-10; ELVIS, Extravasation through Leaky Vasculature and the subsequent Inflammatory cell–mediated Sequestration; LC10, Lethal Concentration for 10% of test organisms; RA, Rheumatoid Arthritis; RES, reticuloendothelial system; LPNs, Lipid–Polymer Hybrid Nanoparticles; DAPI, 4′,6-diamidino-2-phenylindole; IACUC, Institutional Animal Care and Use Committee; PBS, Phosphate-Buffered Saline; OD, Optical Density.

Data Sharing Statement

The data that support the findings of this study are available within the article and its Supplementary Material.

Ethics Approval and Informed Consent

Thirty male Sprague–Dawley rats (6-weeks old, 165–210 g) (accession number: 2022101305) were procured from the Experimental Animal Center of Heilongjiang University of Chinese Medicine (animal certificate: SYXK [black] 2022-009). Rats were acclimated for 1 week prior to experimentation. All studies were approved by the Institutional Animal Care and Use Committee (IACUC) of Heilongjiang University of Chinese Medicine and were conducted in accordance with the National Laboratory Animal Management Regulations and the principles of experimental animal protection.

Acknowledgments

The authors would like to thank the staff and postgraduate students at Heilongjiang University of Chinese Medicine for their assistance in conducting pharmacy research.

Author Contributions

All authors made a significant contribution to the work reported, whether that is in the conception, study design, execution, acquisition of data, analysis and interpretation, or in all these areas; took part in drafting, revising or critically reviewing the article; gave final approval of the version to be published; have agreed on the journal to which the article has been submitted; and agree to be accountable for all aspects of the work.

Funding

This research was supported by the National Natural Science Foundation of China [grant numbers 82074271, 81603418], Support Program for Outstanding Young Academic Leaders of Heilongjiang University of Chinese Medicine, [grant number 15041180106], Funds for the Reform and Development of Local Universities Supported by the Central Government of Provincial Undergraduate Universities in Heilongjiang Province [grant number 2020YQ05], and the Heilongjiang Touyan Innovation Team Program.

Disclosure

The authors report no conflicts of interest in this work.

References

1. Anita C, Munira M, Mural Q, Shaily L. Topical nanocarriers for management of rheumatoid arthritis: a review. *Biomed Pharmacother*. 2021;141:111880. doi:10.1016/j.biopha.2021.111880
2. McInnes IB, Schett G. Pathogenetic insights from the treatment of rheumatoid arthritis. *Lancet*. 2017;389:2328–2337. doi:10.1016/S0140-6736(17)31472-1
3. Conran CA, Moreland LW. A review of biosimilars for rheumatoid arthritis. *Curr Opin Pharmacol*. 2022;64:102234. doi:10.1016/j.coph.2022.102234
4. Zhang S, Zhang M, Li X, et al. Nano-based co-delivery system for treatment of rheumatoid arthritis. *Molecules*. 2022;27:5973. doi:10.3390/molecules27185973
5. Huang J, Fu X, Chen X, Li Z, Huang Y, Liang C. Promising therapeutic targets for treatment of rheumatoid arthritis. *Front Immunol*. 2021;12:686155. doi:10.3389/fimmu.2021.686155
6. Yang M, Ding J, Feng X, et al. Scavenger receptor-mediated targeted treatment of collagen-induced arthritis by dextran sulfate-methotrexate prodrug. *Theranostics*. 2017;7:97–105. doi:10.7150/thno.16844
7. Zhao Y, Jiang C, He J, et al. Multifunctional dextran sulfate-coated reconstituted high density lipoproteins target macrophages and promote beneficial antiatherosclerotic mechanisms. *Bioconjug Chem*. 2017;28:438–448. doi:10.1021/acs.bioconjchem.6b00600

8. Liu X, Wang Z, Qian H, et al. Natural medicines of targeted rheumatoid arthritis and its action mechanism. *Front Immunol*. 2022;13:945129. doi:10.3389/fimmu.2022.945129
9. Zhang L, Wei W. Anti-inflammatory and immunoregulatory effects of paeoniflorin and total glucosides of paeony. *Pharmacol Ther*. 2020;207:107452. doi:10.1016/j.pharmthera.2019.107452
10. Wang DD, Jiang MY, Wang W, et al. Paeoniflorin-6′-O-benzene sulfonate down-regulates CXCR4-Gβγ-PI3K/AKT mediated migration in fibroblast-like synoviocytes of rheumatoid arthritis by inhibiting GRK2 translocation. *Biochem Biophys Res Commun*. 2020;526:805–812. doi:10.1016/j.bbrc.2020.03.164
11. Huang L, Hu S, Shao M, Wu X, Zhang J, Cao G. Combined Cornus officinalis and Paeonia lactiflora pall therapy alleviates rheumatoid arthritis by regulating synovial apoptosis via AMPK-mediated mitochondrial fission. *Front Pharmacol*. 2021;12:639009. doi:10.3389/fphar.2021.639009
12. Jia XY, Chang Y, Sun XJ, et al. Regulatory effects of paeoniflorin-6′-O-benzene sulfonate (CP-25) on dendritic cells maturation and activation via PGE2-EP4 signaling in adjuvant-induced arthritic rats. *Inflammopharmacology*. 2019;27:997–1010. doi:10.1007/s10787-019-00575-8
13. Zhou YX, Gong XH, Zhang H, Peng C. A review on the pharmacokinetics of paeoniflorin and its anti-inflammatory and immunomodulatory effects. *Biomed Pharmacother*. 2020;130:110505. doi:10.1016/j.biopha.2020.110505
14. Shu JL, Zhang XZ, Han L, et al. Paeoniflorin-6′-O-benzene sulfonate alleviates collagen-induced arthritis in mice by downregulating BAFF-TRAF2-NF-κB signaling: comparison with biological agents. *Acta Pharmacol Sin*. 2019;40:801–813. doi:10.1038/s41401-018-0169-5
15. Pang J, Xing H, Sun Y, Feng S, Wang S. Non-small cell lung cancer combination therapy: hyaluronic acid modified, epidermal growth factor receptor targeted, pH sensitive lipid-polymer hybrid nanoparticles for the delivery of erlotinib plus bevacizumab. *Biomed Pharmacother*. 2020;125:109861. doi:10.1016/j.biopha.2020.109861
16. Mohanty A, Uthaman S, Park IK. Utilization of polymer-lipid hybrid nanoparticles for targeted anti-cancer therapy. *Molecules*. 2020;25:4377. doi:10.3390/molecules25194377
17. Yang SC, Bhide M, Crispe IN, Pierce RH, Murthy N. Polyketal copolymers: a new acid-sensitive delivery vehicle for treating acute inflammatory diseases. *Bioconjug Chem*. 2008;19:1164–1169. doi:10.1021/bc700442g
18. Zheng X, Yu X, Wang C, et al. Targeted co-delivery biomimetic nanoparticles reverse macrophage polarization for enhanced rheumatoid arthritis therapy. *Drug Deliv*. 2022;29:1025–1037. doi:10.1080/10717544.2022.2057616
19. Somasuntharam I, Boopathy AV, Khan RS, et al. Delivery of Nox2-NADPH oxidase siRNA with polyketal nanoparticles for improving cardiac function following myocardial infarction. *Biomaterials*. 2013;34:7790–7798. doi:10.1016/j.biomaterials.2013.06.051
20. Zhao YP, Han JF, Zhang FY, et al. Flexible nano-liposomes-based transdermal hydrogel for targeted delivery of dexamethasone for rheumatoid arthritis therapy. *Drug Deliv*. 2022;29:2269–2282. doi:10.1080/10717544.2022.2096718
21. Zhang Y, Xia Q, Wang J, Zhuang K, Jin H, Liu K. Progress in using zebrafish as a toxicological model for traditional Chinese medicine. *J Ethnopharmacol*. 2022;282:114638. doi:10.1016/j.jep.2021.114638
22. Howe K, Clark MD, Torroja CF, et al. The zebrafish reference genome sequence and its relationship to the human genome. *Nature*. 2013;496:498–503. doi:10.1038/nature12111
23. Chen J, Li J, Chen J, et al. Treatment of collagen-induced arthritis rat model by using Notch signalling inhibitor. *J Orthop Translat*. 2021;28:100–107. doi:10.1016/j.jot.2021.01.003
24. Wei SJ, Zhang Q, Xiang YJ, et al. Guizhi-Shaoyao-Zhimu decoction attenuates bone erosion in rats that have collagen-induced arthritis via modulating NF-κB signalling to suppress osteoclastogenesis. *Pharm Biol*. 2021;59:262–274. doi:10.1080/13880209.2021.1876100
25. Wang Q, Jiang J, Chen W, Jiang H, Zhang Z, Sun X. Targeted delivery of low-dose dexamethasone using PCL-PEG micelles for effective treatment of rheumatoid arthritis. *J Control Release*. 2016;230:64–72. doi:10.1016/j.jconrel.2016.03.035
26. Shafique M, Ur Rehman M, Kamal Z, et al. Formulation development of lipid polymer hybrid nanoparticles of doxorubicin and its in-vitro, in-vivo and computational evaluation. *Front Pharmacol*. 2023;14:1025013. doi:10.3389/fphar.2023.1025013
27. Bangera PD, Kara DD, Tanvi K, Tippavajhala VK, Rathnanand M. Highlights on cell-penetrating peptides and polymer-lipid hybrid nanoparticle: overview and therapeutic applications for targeted anticancer therapy. *AAPS Pharm Sci Tech*. 2023;24:124. doi:10.1208/s12249-023-02576-x
28. Huang C, Wang J, Liu H, et al. Ketone body β-hydroxybutyrate ameliorates colitis by promoting M2 macrophage polarization through the STAT6-dependent signaling pathway. *BMC Med*. 2022;20:148. doi:10.1186/s12916-022-02352-x
29. Van den Bossche J, Baardman J, Otto NA, et al. Mitochondrial dysfunction prevents repolarization of inflammatory macrophages. *Cell Rep*. 2016;17:684–696. doi:10.1016/j.celrep.2016.09.008
30. Afrin S, Gasparrini M, Forbes-Hernández TY, et al. Protective effects of Manuka honey on LPS-treated RAW 264.7 macrophages. Part 1: enhancement of cellular viability, regulation of cellular apoptosis and improvement of mitochondrial functionality. *Food Chem Toxicol*. 2018;121:203–213. doi:10.1016/j.fct.2018.09.001
31. Huang H, Chen H, Yao Y, Lou X. Branched-chain amino acids supplementation induces insulin resistance and pro-inflammatory macrophage polarization via INFGR1/JAK1/STAT1 signal pathway. *Mol Med*. 2024;30:149. doi:10.1186/s10020-024-00894-9
32. Luo X, Wang X, Huang S, et al. Paeoniflorin ameliorates experimental colitis by inhibiting gram-positive bacteria-dependent MDP-NOD2 pathway. *Int Immunopharmacol*. 2021;90:107224. doi:10.1016/j.intimp.2020.107224
33. Liu F, Zhang X, Ling P, et al. Immunomodulatory effects of xanthan gum in LPS-stimulated RAW 264.7 macrophages. *Carbohydr Polym*. 2017;169:65–74. doi:10.1016/j.carbpol.2017.04.003
34. Cao Y, Xiong J, Guan X, et al. Paeoniflorin suppresses kidney inflammation by regulating macrophage polarization via KLF4-mediated mitophagy. *Phytomedicine*. 2023;116:154901. doi:10.1016/j.phymed.2023.154901
35. Chen X, Miao J, Wang H, et al. The anti-inflammatory activities of Ainsliaea fragrans Champ. extract and its components in lipopolysaccharide-stimulated RAW264.7 macrophages through inhibition of NF-κB pathway. *J Ethnopharmacol*. 2015;170:72–80. doi:10.1016/j.jep.2015.05.004
36. Lai YS, Hsu WH, Huang JJ, Wu SC. Antioxidant and anti-inflammatory effects of pigeon pea (Cajanus cajan L.) extracts on hydrogen peroxide- and lipopolysaccharide-treated RAW264.7 macrophages. *Food Funct*. 2012;3:1294–1301. doi:10.1039/c2fo30120b
37. Wang Q, Jiang H, Li Y, et al. Targeting NF-kB signaling with polymeric hybrid micelles that co-deliver siRNA and dexamethasone for arthritis therapy. *Biomaterials*. 2017;122:10–22. doi:10.1016/j.biomaterials.2017.01.008
38. Grillet B, Pereira RVS, Van Damme J, Abu El-Asrar A, Proost P, Opdenakker G. Matrix metalloproteinases in arthritis: towards precision medicine. *Nat Rev Rheumatol*. 2023;19:363–377. doi:10.1038/s41584-023-00966-w